Chiral symmetry breaking of a double-stranded helical chain through bend-writhe coupling

Tomohiro Yanao*
Department of Applied Mechanics and Aerospace Engineering, Waseda University, Tokyo 169-8555, Japan

Kenichi Yoshikawa†
Faculty of Life and Medical Sciences, Doshisha University, Kyoto 610-0394, Japan

(Received 21 April 2014; published 26 June 2014)

This paper explores asymmetric elasticity of a double-stranded helical chain, which serves as a minimal model of biopolymers. The model consists of two elastic chains that mutually intertwine in a right-handed manner, forming a double-stranded helix. A simple numerical experiment for structural relaxation, which reduces the total elastic energy of the model monotonically without thermal fluctuations, reveals possible asymmetric elasticity inherent in the helical chain. It is first shown that a short segment of the double-stranded helical chain has a tendency to unwind when it is bent. It is also shown that a short segment of the helical chain has a tendency to writhe in the left direction upon bending. This tendency gives rise to a propensity for a longer segment of the chain to form a left-handed superhelix spontaneously upon bending. Finally, this propensity of the helical chain to form a left-handed superhelix is proposed to be a possible origin of the uniform left-handed wrapping of DNA around nucleosome core particles in nature. The results presented here could provide deeper insights into the roles and significance of helical chirality of biopolymers.

DOI: 10.1103/PhysRevE.89.062713 PACS number(s): 87.14.gk, 87.15.A−, 87.15.B−, 87.15.La

I. INTRODUCTION

Helical motifs are ubiquitous among biopolymers at various scales. Examples include the double-stranded helix of DNA and the α helix of proteins. At larger scales, actin filaments and microtubules are also helical, i.e., helical aggregates of biopolymers. It is of fundamental interest to explore cross-correlations between helical motifs of biopolymers at smaller scales and those at larger scales. One of the most prominent examples where helical motifs appear at various scales is the chromatin [1,2], the packaging architecture of DNA in a eukaryotic cell nucleus. Chromatin indeed appears as a hierarchical "nest" of helical motifs of DNA, although many of its structural details still remain unknown. It is thereby an important challenge to understand the essential designing principles that underlie both the local and global structures of chromatin [3–9].

Given the ubiquity of helical motifs of biopolymers, *helical chirality* is an intriguing property that can underlie the hierarchical organization and dynamics of biopolymers. For example, both the double-stranded helix of the regular B-form DNA and the α helix of proteins are right handed. It is naturally expected that the right-handed helical chirality of these biopolymers gives rise to unique elastic properties that differ markedly from a simple wormlike chain without helical chirality. Indeed, it has been shown experimentally that the twisting stiffness of DNA is asymmetric with respect to the right and left twist [10–12]. It has also been shown experimentally that stretching and twisting of DNA are coupled in an asymmetric and nontrivial manner [13–15]. Marko and Siggia [16] have theoretically argued that DNA unwinds upon bending as a result of an asymmetric coupling between bending and twisting.

An interesting question along this line is whether and how such local asymmetric elasticity of biopolymers rules higher-order structures. Recent studies have revealed some important links between local asymmetric elasticity of biopolymers and their higher-order structures. Kulić *et al.* [17] theoretically proposed that toroidal condensates of DNA relaxes bending energy by twisting its body through the bend-twist coupling and discussed the significance of this effect in the plectonemic supercoiling of the genomes of phages. Velichko *et al.* [18,19] showed numerically that the number of double-helical turns affects the conformation of adsorbed DNA on a surface and changes the scaling properties of DNA. Besteman *et al.* [20] found via magnetic tweezers experiments that the profile of the condensation force of DNA depends on the direction of imposed twist. Dobrovolskaia *et al.* [21] revealed the significance of applied torsional stresses on linker DNA in nucleosome arrays. Higuchi *et al.* [22] showed numerically that torsional stress on DNA can induce a wrapping-unwrapping transition around nucleosome core particles. It is also known that the helical chirality of the DNA double strand is responsible for an asymmetric (chiral) interaction between DNA molecules, giving rise to the chiral cholesteric-like assemblies of DNA [23,24].

In the present study, we investigate the asymmetric nature of the couplings among bending, twisting, and writhing of a double-stranded helical chain at a coarse-grained level. We explore whether such an asymmetric nature can rule the chirality of higher-order structures, such as superhelices of biopolymers. In the example of DNA, one of the most important superhelical structures is the wrapped structure of a nucleosome [1–4], a fundamental repeating unit of chromatin. As is known, DNA wraps around a histone core particle about 1.75 times *in a left-handed manner* to form a nucleosome. The uniformity of the left-handed wrapping of DNA is a remarkable higher-order chirality and is expected to be crucial for the organization and functions of chromatin. Therefore, exploring the link between the asymmetric elasticity of DNA and the

*yanao@waseda.jp
†keyoshik@mail.doshisha.ac.jp

chirality of the wrapped structure of DNA is one of the major objectives of the present study.

The present study is concerned with the minimal and general prerequisites for the selection of chirality in the writhing and wrapping of a double-stranded helical chain. Therefore, our model as well as our numerical analysis employed here is simplified to a great extent: The model polymer consists of two elastic chains that mutually intertwine in a right-handed manner to form a double-stranded helix. The model rules out the difference between the major and minor grooves and the sequence-dependent elasticity of DNA, which have been scrutinized at the atomic or base level in Refs. [25–29], for example. Our present model does not directly treat stacking interactions between bases [30–33] and electrostatic effects [34,35], which are known to be important in structural dynamics of DNA. For the selection of chirality of the wrapped structure of DNA, roles of the size [36,37] and chirality [38,39] of the nucleosome core particles should be of complementary importance. However, we do not deal with these interesting issues in the present study since the present study specifically focuses on the chirality and elasticity of the DNA side. Thus, the nucleosome core particle is modeled as an isotropic sphere in the present study. It is remarkable, however, that despite of the large amount of simplification, our proposed model in this study can reveal an intrinsic propensity of a right-handed helical chain to form a left-handed superhelix and to wrap around a core particle in a left-handed manner.

This paper is organized as follows. In Sec. II, we introduce an elastic model of a double-stranded helical chain with particular attention to DNA. In Sec. III, by taking a short segment of the model chain with 22 base pairs, we study the couplings among its bending, twisting, and writhing. It is shown that the double-stranded helical chain has a general tendency to unwind when it is uniformly bent. It is then shown that the right-handed double-stranded chain has a propensity to writhe in the left direction upon bending. This propensity of the chain to writhe in the left direction can be a basis for the assumption that was introduced in our previous study on chiral selection in DNA wrapping [40]. In Sec. IV, we take a longer segment of the model chain with 78 base paris to study the chirality of the superhelices of DNA. It is shown that a long segment of the chain has a propensity to form a left-handed superhelix when it is bent. We finally propose that this propensity can be a prime factor for the uniform left-handed wrapping of DNA around nucleosome core particles. This paper concludes in Sec. V with some remarks on future directions of research.

II. ELASTIC MODEL OF A DOUBLE-STRANDED HELICAL CHAIN

In this section, we introduce a simplified model of a double-stranded helical chain. This model is of particular interest for the study of asymmetric (chiral) elasticity of biopolymers.

A. Construction of the model

The model consists of two elastic chains that mutually intertwine in a right-handed manner around a central backbone.

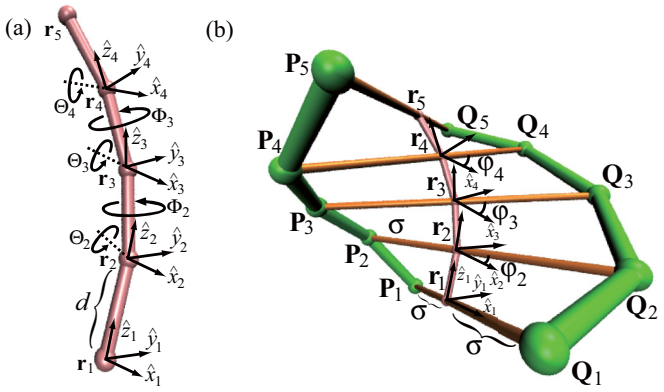

FIG. 1. (Color online) (a) Illustration of the central backbone of the double-stranded helical chain with $N = 5$ base pairs, showing bending angles $\{\Theta_i | i = 2,\ldots,N-1\}$, dihedral angles $\{\Phi_i | i = 2,\ldots,N-2\}$, and local frames $(\hat{\boldsymbol{x}}_i,\hat{\boldsymbol{y}}_i,\hat{\boldsymbol{z}}_i)$. (b) Illustration of the two elastic chains (P chain and Q chain) intertwining around the central backbone. The bridges linking the two chains are also shown, where $\{\varphi_i\}$ are the twist angles measured with respect to the local frames defined in (a). The distance between two adjacent nodal points of the central backbone is fixed to $d = 0.34$ nm. The half length of the bridges is fixed to $\sigma = 1$ nm.

Figure 1(a) illustrates the central backbone of the model, and Fig. 1(b) shows the two elastic chains intertwining around the central backbone for the example of the model with $N = 5$ "base pairs." Since the model is largely based on DNA, we use the term "base pairs" for the links (bridges) between the two chains in Fig. 1(b). As will be clear in the following, the central backbone is merely for the parametrization of the overall conformation of the two chains intertwining around it and does not affect the elastic energy of the system directly.

Conformation of the central backbone is parameterized in the same way as the standard model of polymer chains [41] as follows. The central backbone consists of N successive nodal points, where N corresponds to the number of base pairs of the model. The distance between every two adjacent nodal points is fixed to d [see Fig. 1(a)]. Since d determines the distance between two adjacent base pairs of the chain, we set this parameter to be $d = 0.34$ nm based on the DNA structure [1,2]. Let the position of the i-th nodal point be represented by the three-dimensional vector $\mathbf{r}_i$ $(i = 1,\ldots,N)$. The first nodal point of the backbone is located at the origin of the space without loss of generality, i.e., $\mathbf{r}_1 = (0,0,0)$. We then introduce a three-dimensional orthonormal frame, F_1, which consists of three orthogonal unit vectors of axes $(\hat{\boldsymbol{x}}_1,\hat{\boldsymbol{y}}_1,\hat{\boldsymbol{z}}_1)$ [see Fig. 1(a)]. The $\hat{\boldsymbol{z}}_1$ axis of this frame is set parallel to the vector $\mathbf{r}_2 - \mathbf{r}_1$, which connects the first and the second nodal points. The $\hat{\boldsymbol{y}}_1$ axis is defined to be perpendicular to the $\hat{\boldsymbol{z}}_1$ axis and to lie within the plane spanned by the three nodal points, $\mathbf{r}_1$, $\mathbf{r}_2$, and $\mathbf{r}_3$. The $\hat{\boldsymbol{x}}_1$ axis is defined as $\hat{\boldsymbol{x}}_1 = \hat{\boldsymbol{y}}_1 \times \hat{\boldsymbol{z}}_1$. Thus, the position of the second nodal point is represented as $\mathbf{r}_2 = (0,0,d)$ with respect to the frame F_1.

The second frame F_2 is defined to be the same as the first one, i.e., $(\hat{\boldsymbol{x}}_2,\hat{\boldsymbol{y}}_2,\hat{\boldsymbol{z}}_2) = (\hat{\boldsymbol{x}}_1,\hat{\boldsymbol{y}}_1,\hat{\boldsymbol{z}}_1)$. The third frame F_3 is obtained by rotating F_2 by an angle Θ_2 around the $\hat{\boldsymbol{x}}_2$ axis so the $\hat{\boldsymbol{z}}_2$ axis is parallel to the vector $\mathbf{r}_3 - \mathbf{r}_2$. The fourth frame

F_4 is obtained by rotating the frame F_3 by an angle Φ_2 around the $\hat{\boldsymbol{z}}_3$ axis and then by an angle Θ_3 around the $\hat{\boldsymbol{x}}_3$ axis so the $\hat{\boldsymbol{z}}_3$ axis is parallel to the vector $\mathbf{r}_4 - \mathbf{r}_3$.

Thus, by introducing the matrices,

$$\mathsf{R}_i^{i-1}(\Phi_{i-2},\Theta_{i-1}) \equiv \begin{pmatrix} \cos\Phi_{i-2} & -\sin\Phi_{i-2} & 0 \\ \sin\Phi_{i-2} & \cos\Phi_{i-2} & 0 \\ 0 & 0 & 1 \end{pmatrix} \times \begin{pmatrix} 1 & 0 & 0 \\ 0 & \cos\Theta_{i-1} & -\sin\Theta_{i-1} \\ 0 & \sin\Theta_{i-1} & \cos\Theta_{i-1} \end{pmatrix}, \quad (i = 3,\ldots,N) \tag{1}$$

and a vector $\mathbf{d} = (0,0,d)^T$, the positions of the third and fourth nodal points, $\mathbf{r}_3$ and $\mathbf{r}_4$, are represented, respectively, as

$$\mathbf{r}_3 = \mathbf{r}_2 + \mathsf{R}_3^2(0,\Theta_2)\mathbf{d}, \tag{2}$$

$$\mathbf{r}_4 = \mathbf{r}_3 + \mathsf{R}_3^2(0,\Theta_2)\mathsf{R}_4^3(\Phi_2,\Theta_3)\mathbf{d}. \tag{3}$$

Similarly, the fifth and later nodal points are represented in a general form as

$$\mathbf{r}_i = \mathbf{r}_{i-1} + \mathsf{R}_3^2(0,\Theta_2)\mathsf{R}_4^3(\Phi_2,\Theta_3)\cdots\mathsf{R}_i^{i-1}(\Phi_{i-2},\Theta_{i-1})\mathbf{d}, \quad (i = 5,\ldots,N). \tag{4}$$

Note that the three columns of each matrix $\mathsf{R}_i^{i-1}(\Phi_{i-2},\Theta_{i-1})$ represent the three axes of the i-th frame, F_i, with respect to the $(i-1)$-th frame, F_{i-1}. The angle Θ_i is the bending angle of the backbone at the i-th nodal point, while the angle Φ_i represents the dihedral angle between the plane spanned by the three nodal points $\{\mathbf{r}_{i-1},\mathbf{r}_i,\mathbf{r}_{i+1}\}$ and the plane spanned by the three nodal points $\{\mathbf{r}_i,\mathbf{r}_{i+1},\mathbf{r}_{i+2}\}$. The ranges of these angles are

$$0^\circ \leqslant \Theta_i \leqslant 180^\circ, \quad -180^\circ \leqslant \Phi_i < 180^\circ. \tag{5}$$

Thus, the configuration of the central backbone of N nodal points is determined uniquely by the $N-2$ bending angles $\{\Theta_i | i = 2,\ldots,N-1\}$ and the $N-3$ dihedral angles $\{\Phi_i | i = 2,\ldots,N-2\}$.

Next, we introduce the two elastic chains that intertwine around the central backbone in a right-handed manner. These two chains, called the P chain and the Q chain, can be regarded as the sugar-phosphate chains of DNA and are mutually bonded with the rigid bridges representing hydrogen-bonded base pairs [see Fig. 1(b)]. Each of the P and Q chains consists of N nodal points connected with $N-1$ harmonic springs to one another. Positions of these nodal points with respect to the space-fixed frame are represented by the three-dimensional vectors $\{\mathbf{P}_i | i = 1,\ldots,N\}$ for the P chain and $\{\mathbf{Q}_i | i = 1,\ldots,N\}$ for the Q chain, respectively. The first nodal points of the two chains, $\mathbf{P}_1$ and $\mathbf{Q}_1$, are placed so the center of these two points coincides with the point $\mathbf{r}_1$ and the vector $(\mathbf{Q}_1 - \mathbf{P}_1)$ is parallel to the $\hat{\boldsymbol{x}}_1$ axis of the frame F_1. Since the point $\mathbf{r}_1$ and the $\hat{\boldsymbol{x}}_1$ axis are fixed to the space, the points $\mathbf{P}_1$ and $\mathbf{Q}_1$ are also fixed to the space.

The points $\mathbf{P}_i$ and $\mathbf{Q}_i$ (for $i = 1,\ldots,N$) are bonded with a rigid bridge, whose length is fixed to 2σ. Since this bridge represents the hydrogen-bonded base pair for DNA and determines the diameter of the model chain, we set the value of σ to be $\sigma = 1$ nm [1,2]. The vector $(\mathbf{Q}_i - \mathbf{P}_i)$ $(i = 2,\ldots,N)$ can rotate rigidly with its center fixed to the nodal point of the central backbone $\mathbf{r}_i$. The rotation of the vector $(\mathbf{Q}_i - \mathbf{P}_i)$ is restricted within the plane perpendicular to the $\hat{\boldsymbol{z}}_i$ axis (i.e., within the $\hat{\boldsymbol{x}}_i$-$\hat{\boldsymbol{y}}_i$ plane). The angle between the $\hat{\boldsymbol{x}}_i$ axis and the vector $(\mathbf{Q}_i - \mathbf{P}_i)$ is defined as $\varphi_i (i = 1,\ldots,N)$. Note that $\varphi_1 \equiv 0^\circ$ since the vector $(\mathbf{Q}_1 - \mathbf{P}_1)$ is always parallel to the $\hat{\boldsymbol{x}}_1$ axis. Thus, by introducing the three-dimensional vectors $\mathbf{h}_i = (\sigma\cos\varphi_i, \sigma\sin\varphi_i, 0)^T$ $(i = 1,\ldots,N)$, the points $\{\mathbf{P}_i\}$ and $\{\mathbf{Q}_i\}$ are represented with respect to the space-fixed frame as

$$\mathbf{P}_2 = \mathbf{r}_2 - \mathbf{h}_2, \tag{6}$$

$$\mathbf{Q}_2 = \mathbf{r}_2 + \mathbf{h}_2, \tag{7}$$

$$\mathbf{P}_3 = \mathbf{r}_3 - \mathsf{R}_3^2(0,\Theta_2)\mathbf{h}_3, \tag{8}$$

$$\mathbf{Q}_3 = \mathbf{r}_3 + \mathsf{R}_3^2(0,\Theta_2)\mathbf{h}_3, \tag{9}$$

$$\mathbf{P}_i = \mathbf{r}_i - \mathsf{R}_3^2(0,\Theta_2)\mathsf{R}_4^3(\Phi_2,\Theta_3)\cdots \times \mathsf{R}_i^{i-1}(\Phi_{i-2},\Theta_{i-1})\mathbf{h}_i \quad (i = 4,\ldots,N), \tag{10}$$

$$\mathbf{Q}_i = \mathbf{r}_i + \mathsf{R}_3^2(0,\Theta_2)\mathsf{R}_4^3(\Phi_2,\Theta_3)\cdots \times \mathsf{R}_i^{i-1}(\Phi_{i-2},\Theta_{i-1})\mathbf{h}_i \quad (i = 4,\ldots,N). \tag{11}$$

In this manner, the angles $\Theta_i (i = 2,\ldots,N-1)$, $\Phi_i (i = 2,\ldots,N-2)$, and $\varphi_i (i = 1,\ldots,N)$ parametrize the conformation of the double-stranded helical chain uniquely. While the angles $\{\Theta_i\}$ and $\{\Phi_i\}$ characterize rather global conformations of the model, i.e., *bend* and *writhe* of the central backbone, the angles $\{\varphi_i\}$ characterize local *twist* of the double-stranded helix. As is evident, the present model incorporates neither the major groove nor minor groove of DNA [26] nor the structural differences of different base pairs [27].

B. Equilibrium conformation and energy functions

We incorporate here elastic energies into the double-stranded helical chain based on the coordinates introduced in the previous subsection. For this sake, we first define the equilibrium conformation of the model, which corresponds to the minimum of the total elastic energy. We assume that the backbone of the model chain is straight, i.e., $\Theta_i = 0^\circ$ for all i, at the equilibrium conformation as shown in Fig. 2(a) for an example of the system with $N = 5$ base pairs. We also assume that every two adjacent bridges form the same constant angle φ_0 at the equilibrium conformation when the bridges are vertically projected onto a plane perpendicular to the central backbone of the chain as shown in Fig. 2(b). Thus, each φ_i takes the value

$$\varphi_i = (i-1)\varphi_0 \quad (i = 1,\ldots,N), \tag{12}$$

at the equilibrium conformation. Here it should be noted that all $\hat{\boldsymbol{x}}_i$-$\hat{\boldsymbol{y}}_i$ planes are parallel at the equilibrium conformation because of the condition $\Theta_i = 0^\circ$ for all i. The actual value of φ_0 is set to $\varphi_0 \equiv 36^\circ$. This is based on the fact that the double-stranded helix of DNA completes one cycle per every

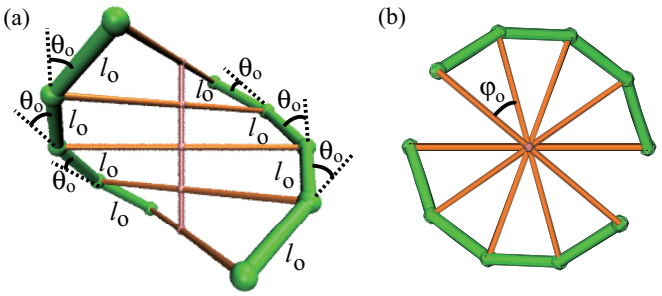

FIG. 2. (Color online) Equilibrium conformation of the double-stranded helical chain with five base pairs. Panel (a) shows a side view, where θ_0 is the equilibrium bending angle at each nodal point of the two elastic chains and l_0 is the equilibrium length of the bonds in the two elastic chains. Panel (b) shows a cross-sectional view of the double-stranded helical chain at the equilibrium conformation, where $\varphi_0 \equiv 36^\circ$ is the equilibrium angle between two adjacent bridges of base pairs projected onto the cross section.

$360^\circ/36^\circ = 10$ base pairs approximately. The positive value of φ_0 assures that the double-stranded helical chain is right handed as in B-form DNA and actin filaments.

All the contributions to the elastic energy of the system originate from the bonding, i.e., stretching and contraction, and the bending of each of the two sugar-phosphate chains, P chain and Q chain. That is, the elastic energy does not depend directly on the central backbone of the model. This is why the central backbone is just for the parametrization of the P chain and Q chain as noted at the beginning of this section.

As for the bonding energy, we adopt a simple harmonic potential to every bond between two adjacent nodal points of the P and Q chains. Therefore, the sum of the bonding energies of the two chains is written as

$$\frac{E_{\rm bond}}{k_{\rm B}T} = \sum_{i=1}^{N-1} \frac{1}{2} k_{\rm bond}(|\mathbf{P}_{i+1} - \mathbf{P}_i| - l_0)^2 + \sum_{i=1}^{N-1} \frac{1}{2} k_{\rm bond}(|\mathbf{Q}_{i+1} - \mathbf{Q}_i| - l_0)^2, \quad (13)$$

where the first sum is the bonding energy of the P chain and the second sum is that of the Q chain. In the present study, energies are measured with respect to $k_{\rm B}T$, where $k_{\rm B}$ is the Boltzmann constant and T is temperature. In Eq. (13), $k_{\rm bond}$ is the force constant for bonding and is common to all the bonds in the P chain and Q chain. l_0 is the equilibrium distance of all the bonds in the P chain and Q chain.

Harmonic potential is also used for the bending energy of the P and Q chains at each nodal point. Thus, the sum of the bending energies of the two chains is written as

$$\frac{E_{\rm bend}}{k_{\rm B}T} = \sum_{i=2}^{N-1} \frac{1}{2} k_{\rm bend}\left(\theta_i^{(P)} - \theta_0\right)^2 + \sum_{i=2}^{N-1} \frac{1}{2} k_{\rm bend}\left(\theta_i^{(Q)} - \theta_0\right)^2, \quad (14)$$

where $\theta_i^{(P)}$ and $\theta_i^{(Q)}$ are the bending angles of the P and Q chains at the respective nodal points. They are defined by

$$\theta_i^{(P)} = \cos^{-1}\left(\frac{\mathbf{P}_i - \mathbf{P}_{i-1}}{|\mathbf{P}_i - \mathbf{P}_{i-1}|} \cdot \frac{\mathbf{P}_{i+1} - \mathbf{P}_i}{|\mathbf{P}_{i+1} - \mathbf{P}_i|}\right), \quad (i = 2, \ldots, N-1), \quad (15)$$

$$\theta_i^{(Q)} = \cos^{-1}\left(\frac{\mathbf{Q}_i - \mathbf{Q}_{i-1}}{|\mathbf{Q}_i - \mathbf{Q}_{i-1}|} \cdot \frac{\mathbf{Q}_{i+1} - \mathbf{Q}_i}{|\mathbf{Q}_{i+1} - \mathbf{Q}_i|}\right), \quad (i = 2, \ldots, N-1). \quad (16)$$

In Eq. (14), θ_0 is the equilibrium value for the bending angles, $\theta_i^{(P)}$ and $\theta_i^{(Q)}$. Since the P and Q chains have a natural bending angle at the respective nodal points already at the equilibrium conformation of the system [see Fig. 2(a)], the equilibrium bending angle θ_0 is not zero.

By inspection of the equilibrium conformation shown in Fig. 2, the actual values of the equilibrium bond distance l_0 in Eq. (13) and the equilibrium bending angle θ_0 in Eq. (14) are determined uniquely in terms of the parameters σ, d, and φ_0 as

$$\theta_0 = \cos^{-1}\left[\frac{2\sigma^2 \cos\varphi_0(1 - \cos\varphi_0) + d^2}{2\sigma^2(1 - \cos\varphi_0) + d^2}\right], \quad (17)$$

$$l_0 = \sqrt{2\sigma^2(1 - \cos\varphi_0) + d^2}, \quad (18)$$

which give $\theta_0 = 31.4^\circ$ and $l_0 = 0.705$ nm, respectively, for $\sigma = 1$ nm, $d = 0.34$ nm, and $\varphi_0 = 36^\circ$. The total elastic energy of the system is the sum of Eq. (13) and Eq. (14),

$$E = E_{\rm bond} + E_{\rm bend}, \quad (19)$$

which takes the minimum value, $E = 0$, at the equilibrium conformation of the system, where $|\mathbf{P}_{i+1} - \mathbf{P}_i| = |\mathbf{Q}_{i+1} - \mathbf{Q}_i| = l_0$ and $\theta_i^{(P)} = \theta_i^{(Q)} = \theta_0$ for all i.

So far, we have determined all the parameter values of the model chain based on the structural data on DNA except for the force constant for bonding, $k_{\rm bond}$, and that for bending, $k_{\rm bend}$. Since no direct experimental data are available for these two parameters, we adopt $k_{\rm bond} = 100\,{\rm nm}^{-2}$ and $k_{\rm bend} = 100\,{\rm rad}^{-2}$ unless otherwise noted. With these parameter values, the persistence length [42,43] of the present model is considered to be about 10–15 nm as is estimated from the total energy of the system upon bending (see the Appendix for the estimation of the persistence length of the model). Although this value is smaller than the persistence length of real DNA (around 50 nm), it is expected that the physical characteristics of DNA with a large difference between the persistence length and the diameter holds under such parametrization. In the present model, a larger value of $k_{\rm bend}$ gives a larger persistence length in general. In the following sections, we occasionally change these parameter values in order to show that the basic propensities of the model are qualitatively independent of the details of these parameter values.

III. COUPLINGS AMONG BENDING, TWISTING, AND WRITHING OF A SHORT SEGMENT OF THE DOUBLE-STRANDED HELICAL CHAIN

In this section, we investigate the couplings among bending, twisting, and writhing of a short segment of the double-

stranded helical chain with $N = 22$ base pairs. First, it is shown that the chain tends to *unwind* when it is uniformly bent. It is also shown that the chain tends to *writhe* in an asymmetric manner *in the left direction* when it reverts back from a bent conformation to the equilibrium straight conformation.

A. Asymmetric coupling between bending and twisting

We first investigate the effect of bending on the twist of the double-stranded helical chain. We take up a short segment of the chain with $N = 22$ base pairs and set the initial conformation so the central backbone of the model is uniformly bent and forms a planar arc as shown in Fig. 3(a). (In this figure and hereafter, the central backbone of the chain is not shown.) Specifically, we set all the bending angles of the central backbone as $\Theta_i = 10^\circ$ (for $i = 2, \ldots, N-1$) and all the dihedral angles of the central backbone as $\Phi_i = 0^\circ$ (for $i = 2, \ldots, N-2$). Initial twisting angles of the double strand $\{\varphi_i\}$ are set to the values at the equilibrium conformation of the system, i.e., $\varphi_i = (i-1)\varphi_0$ (for $i = 1, \ldots, N$) as prescribed in Eq. (12). The length of the respective bonds in the P and Q chains, $|\mathbf{P}_{i+1} - \mathbf{P}_i|$ and $|\mathbf{Q}_{i+1} - \mathbf{Q}_i|$, and the respective bending angles of these two chains defined in Eq. (15) and Eq. (16) are adjusted in accordance with the above-mentioned initial conformation. This initial conformation induces an elastic stress, i.e., nonzero total energy, in the system through Eq. (13) and Eq. (14). In the real world, this initial conformation may be realized when a double-stranded helical chain is abruptly bent due to a strong force before the twisting degrees of freedom relax.

Starting from this initial conformation, we let all the twisting angles $\{\varphi_i\}$ of the system relax by gradually and monotonically lowering the total elastic energy of the system. Throughout this relaxation process, all the bending angles and all the dihedral angles of the central backbone are fixed to the initial values, i.e., $\Theta_i = 10^\circ$ and $\Phi_i = 0^\circ$ (for all i). That is, the central backbone of the double-stranded chain is fixed to the uniformly bent conformation without writhe throughout this relaxation process.

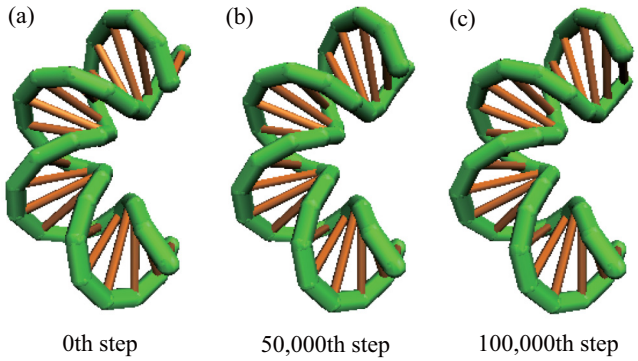

FIG. 3. (Color online) Snapshots of the double-stranded helical chain with $N = 22$ base pairs in the course of structural relaxation under the condition that the backbone of the chain is uniformly bent and fixed to a planar-arc conformation. Panel (a) is the initial conformation, while panels (b) and (c) are the conformations at the 50 000th and 100 000th steps in the relaxation process, respectively.

The numerical procedure for the structural relaxation employed here is essentially a Monte Carlo method with zero temperature: Suppose that we have a "current" conformation of the double-stranded helical chain. Then, one of the twisting angles, e.g., φ_i, is chosen randomly and replaced with a trial value, $\varphi_i^{\rm try} = \varphi_i + \Delta\varphi$, where $\Delta\varphi$ is a small random number within the range $-0.01^\circ \leqslant \Delta\varphi \leqslant 0.01^\circ$, to yield a trial conformation of the system. Note that this trial conformation slightly differs from the "current" conformation due to the replacement of φ_i with $\varphi_i + \Delta\varphi$. If the total energy of the trial conformation is lower than that of the "current" one, the trial conformation is accepted as a new "current" conformation. If the trial conformation has higher total energy than the "current" one, the trial conformation is rejected, and another trial conformation is examined. This procedure is repeated until the total elastic energy of the system converges to a minimum value.

Figure 3 shows the snapshots of the double-stranded helical chain in the course of structural relaxation. As one can see from Figs. 3(a)–3(c), the short segment of the helical chain *unwinds* in the course of this relaxation process. Note that the base pair at the bottom of the pictures in Figs. 3(a)–3(c) is fixed to the space and does not move during the relaxation process. As a result, the lower part of the chain in Figs. 3(a)–3(c) does not change very largely in the relaxation process, while the upper part of the chain unwinds largely.

To be more quantitative, the solid curve in Fig. 4(a) shows the evolution of the total elastic energy of the system, $E = E_{\rm bond} + E_{\rm bend}$ defined in Eq. (19), in the relaxation process of Fig. 3. We confirm that the elastic energy decreases monotonically and approaches an asymptotic value, which corresponds to the minimum of the total elastic energy under the conditions that the backbone is uniformly bent and fixed to the planar-arc conformation. The broken curve in Fig. 4(a) shows the evolution of the bonding energy $E_{\rm bond}$, while the dotted curve shows the evolution of the bending energy $E_{\rm bend}$, respectively. We see from these two curves that the decrease of the total elastic energy is the result of the decrease of the bending energy $E_{\rm bend}$. Indeed, the bonding energy $E_{\rm bond}$ has slightly increased in the structural relaxation. This slight increase of the bonding energy is overwhelmed by the significant decrease of the bending energy.

Figures 4(b) shows the change in the twisting number of the system defined by

$$\mathrm{Tw} = \varphi_N/360^\circ, \tag{20}$$

which is a measure of the number of helical turns in the double-stranded helical chain. It is evident that the twisting number Tw decreases monotonically from $\mathrm{Tw} = 2.1$ to about $\mathrm{Tw} = 2.0$ in the structural relaxation. This confirms that the double-stranded helical chain unwinds in the process of reducing the elastic stress induced by the bending of the chain. This result appears to be consistent with the theoretical prediction of Marko and Siggia [16] that DNA unwinds upon bending.

In order to confirm the robustness and generality of the above propensity of the double-stranded helical chain to unwind upon bending, we carried out the similar numerical experiments to Fig. 3 for different values of the force constants,

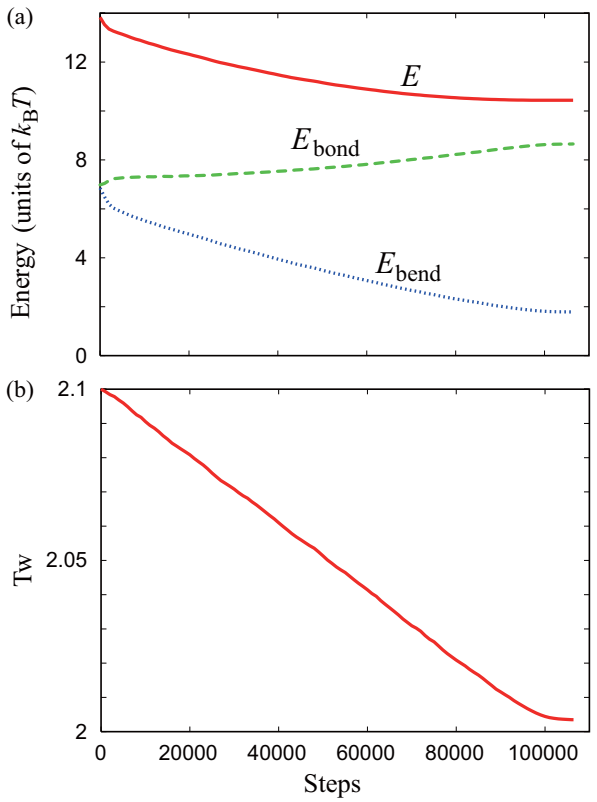

FIG. 4. (Color online) (a) The solid curve shows the evolution of the total elastic energy of the double-stranded helical chain with $N = 22$ base pairs, $E = E_{\rm bond} + E_{\rm bend}$ defined in Eq. (19), in the relaxation process shown in Fig. 3. The broken curve and the dotted curve show the evolution of the bonding energy $E_{\rm bond}$ and the bending energy $E_{\rm bend}$, respectively. (b) Evolution of the twisting number Tw defined in Eq. (20) in the same relaxation process as in (a).

$k_{\rm bond}$ and $k_{\rm bend}$. We used the same double-stranded helical chain as in Fig. 3 with $N = 22$ base pairs. All the bending angles and dihedral angles of the central backbone were fixed to $\Theta_i = 10^\circ$ and $\Phi_i = 0^\circ$ (for all i) respectively throughout the structural relaxation. Figure 5(a) shows the dependence of the difference between initial and final twisting number, ΔTw, on the force constant for bending $k_{\rm bend}$, where the force constant for bonding is fixed to $k_{\rm bond} = 100$ nm^{-2}. We see that the twisting number always decreases in the structural relaxation, i.e., $\Delta{\rm Tw} < 0$, except for the case $k_{\rm bend} = 0$, where ΔTw increases very slightly. As $k_{\rm bend}$ becomes larger, the double-stranded helical chain unwinds to a greater extent upon bending, indicating that the bending stiffness of the two sugar-phophate chains drives the unwinding of the double-stranded helical chain upon bending. Figure 5(b) shows the dependence of ΔTw on the force constant for bonding $k_{\rm bond}$, where the force constant for bending is fixed to $k_{\rm bend} = 100$ nm^{-2}. Again, we see that ΔTw is always negative, indicating the robustness of the unwinding of the double-stranded helical chain upon bending. As $k_{\rm bond}$ becomes larger, the amount of unwinding decreases, indicating that the bond stiffness of the two chains hinders the unwinding of the double-stranded helical chain. The results of Figs. 3(a) and 3(b) clearly confirm that the unwinding of double-stranded helical chain upon bending is a robust and general propensity resulted from the helical structure of the chain.

We next investigate more in detail the mechanism for the unwinding of the double-stranded helical chain upon bending observed above. Figure 6 compares the respective bond lengths and bending angles of the double-stranded helical chain before and after the relaxation process of Fig. 3. In Fig. 6(a), the squares and triangles linked with *solid lines* represent the *initial* lengths of the respective bonds in the P chain or Q chain, $l_i^{(P)} = |\mathbf{P}_{i+1} - \mathbf{P}_i|$ and $l_i^{(Q)} = |\mathbf{Q}_{i+1} - \mathbf{Q}_i|$ ($i = 1, \ldots, 21$). The squares and triangles linked with *broken lines* represent the *final* lengths of the respective bonds in the P chain and Q chain. As can be seen, both at the initial and final conformations, the length of the bonds in the P chain and that in the Q chain change periodically with respect to the bond number i. This periodicity is obviously due to the periodicity of the helical structure of the two chains. One should note here that the equilibrium length of the respective bonds in the P and Q chains is $l_0 = 0.705$ nm. By comparing the solid lines and the broken lines in Fig. 6(a), we see that the final contour lengths of the two chains are shorter and differ more largely from the equilibrium length on average than the initial contour lengths of the two chains. This is why the bonding energy of the two chains slightly increases in the structural relaxation as we have seen in Fig. 4(a). This small increase of the bonding energy can be regarded as a necessary cost for the significant decrease of the bending energy.

Since the bending energy decreases largely in the structural relaxation process as we have seen in Fig. 4(a), we expect that the major driving factor for the unwinding of the double-stranded helical chain upon bending originates from the relaxation of the bending angles of the two constituent chains (P and Q chains). Figure 6(b) compares the initial and the final bending angles of the two chains, $\theta_i^{(P)}$ and $\theta_i^{(Q)}$ ($i = 2, \ldots, 21$), in the relaxation process of Fig. 3. In Fig. 6(b), the squares and triangles linked with the *solid lines* represent the *initial* values of the bending angles of the P chain and Q chain. The squares and triangles linked with *broken lines* represent the *final* values of the bending angles of the P chain and Q chain. Since the equilibrium value for all the bending angles in the P and Q chains is $\theta_0 = 31.4^\circ$ as computed from Eq. (17), we see that almost all the bending angles of the P and Q chains are initially greater than the equilibrium value. This is simply because the bending of the central backbone of the double-stranded helical chain induces additional bending at the respective nodal points of the P and Q chains. Therefore, in the relaxation process, both the P and Q chain deform so as to reduce their bending angles and bring them close to the equilibrium value $\theta_0 = 31.4^\circ$ as much as possible. One can confirm this by comparing the solid lines (initial bending angles) and the broken lines (final bending angles) in Fig. 6(b).

To summarize, the primary factor for the unwinding of the double-stranded helical chain upon bending is in the decrease of the bending angles of the two constituent helical chains (P and Q chains). It has also been revealed that the contour lengths of the two chains decrease in this process, which gives rise to a slight energy cost in the system. In Sec. III C, we analytically show that such decrease of the contour length of the two chains induced by the decrease of the bending angles indeed gives rise to the unwinding of the double-stranded helical chain.

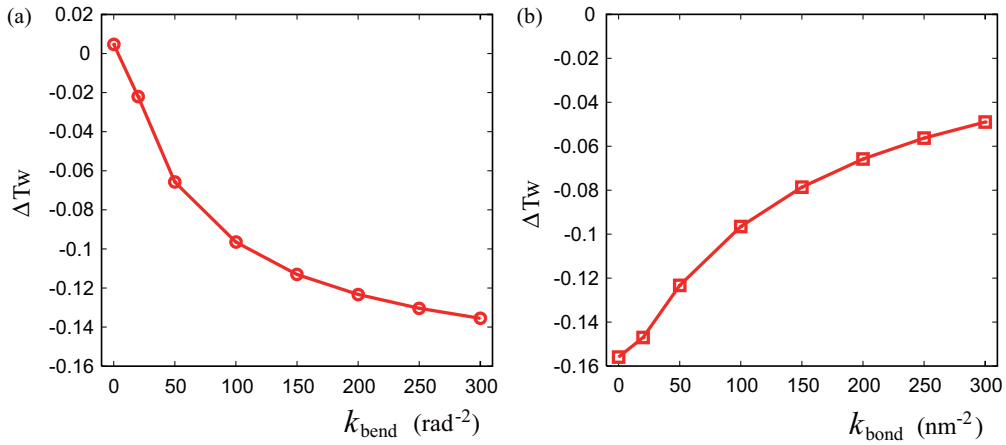

FIG. 5. (Color online) The vertical axis, ΔTw, represents the difference between initial and final twisting numbers of the double-stranded helical chain with $N = 22$ base pairs in the structural relaxation simulation. Panel (a) shows the dependence of ΔTw on the force constant for bending, k_{bend}, where the force constant for bonding is fixed to $k_{bond} = 100$ nm^{-2}. Panel (b) shows the dependence of ΔTw on the force constant for bonding, k_{bond}, where the force constant for bending is fixed to $k_{bend} = 100$ rad^{-2}.

B. Asymmetric coupling between bending and writhing

We study here the coupling between bending and writhing of the double-stranded helical chain by using the same model with $N = 22$ base pairs as in Sec. III A. We begin with exactly the same initial conditions of the chain as in the previous subsection shown in Fig. 3(a). That is, all the initial bending angles of the central backbone are set to $\Theta_i = 10^\circ$ (for $i = 2, \ldots, N-1$), and all the dihedral angles of the central backbone are set to $\Phi_i = 0^\circ$ (for $i = 2, \ldots, N-2$). Initial twisting angles of the double strand $\{\varphi_i\}$ are set according to Eq. (12). Respective initial bond lengths in the P and Q chains, $|\mathbf{P}_{i+1} - \mathbf{P}_i|$ and $|\mathbf{Q}_{i+1} - \mathbf{Q}_i|$, as well as the respective initial bending angles of these two chains defined in Eq. (15) and Eq. (16), are adjusted in accordance with the above conditions.

In the numerical experiments of Sec. III A, the central backbone of the double-stranded helical chain are fixed and only the twisting angles $\{\varphi_i\}$ could relax. On the other hand, in this subsection, we let the double-stranded helical chain relax totally freely. That is, not only the twisting angles $\{\varphi_i\}$ but also the bending angles $\{\Theta_i\}$ and the dihedral angles $\{\Phi_i\}$ of the central backbone can relax freely. With this numerical experiment, one can investigate not only the coupling between bending and twisting but also the coupling between bending and writhing of the double-stranded helical chain.

Numerical procedure for the structural relaxation is similar to the one in the previous subsection. However, in this subsection, not only one of the twisting angles φ_i but also one of the bending angles Θ_i and one of the dihedral angles Φ_i of the central backbone are chosen randomly and replaced with trial values as $\varphi_i^{\text{try}} = \varphi_i + \Delta\varphi$, $\Theta_i^{\text{try}} = \Theta_i + \Delta\Theta$, and $\Phi_i^{\text{try}} = \Phi_i + \Delta\Phi$ to obtain a trial conformation, where $\Delta\varphi$, $\Delta\Theta$, and $\Delta\Phi$ are small random numbers satisfying $-0.01^\circ \leqslant \Delta\varphi \leqslant 0.01^\circ$, $-0.005^\circ \leqslant \Delta\Theta \leqslant 0.005^\circ$, and $-0.01^\circ \leqslant \Delta\Phi \leqslant 0.01^\circ$. If the trial conformation has lower energy than the "current" conformation, the trial conformation is accepted as a new "current" conformation. If the trial conformation has higher elastic energy than the "current" one, the trial conformation is rejected, and another trial conformation is examined. This procedure is repeated until the total elastic energy of the system converges to a minimum value.

Figure 7 shows a typical relaxation process of the double-stranded helical chain, where it took about 87 000 steps for the total energy of the system to converge to a minimum value. Figure 7(a) is the initial conformation of the model, which is the same as Fig. 3(a) observed from a different viewpoint. As the system relaxes, the initial bent conformation changes to the straight conformation [Fig. 7(d)], which is the equilibrium conformation. Importantly, the double-stranded helical chain *writhes in the left direction* at the early stage of the relaxation process, as is seen in Fig. 7(b). This propensity of the double-stranded helical chain to writhe in the left direction is expected to modulate its apparent stretchability in a significant manner.

In order to observe the writhing of the double-stranded helical chain more clearly, it is useful to highlight the behavior of the central backbone of the double-stranded helical chain. Thus, we pick up the 1st, 8th, 15th, and 22nd nodal points of the central backbone of the double-stranded helical chain and connect them together in this order with three straight sticks to form a single chain. This single chain can be regarded as a coarse-grained system of the original double-stranded helical chain. Figures 8(a)–8(d) show the change in the conformation of this coarse-grained system for the same relaxation process as in Fig. 7. We see that the coarse-grained system forms a planar bent conformation at the beginning (0th step) and writhes in the left direction before it finally relaxes to the straight conformation. Figure 8(e) shows the evolution of the dihedral angle of the coarse-grained system, Ψ, in this relaxation process. This dihedral angle Ψ is initially zero at the 0th step reflecting the planar configuration of the central backbone of the double-stranded helical chain. Then Ψ quickly decreases to about $\Psi = -11.5^\circ$ in the first 11 000 steps and gradually reverts back to zero. The negative value of the dihedral angle, $\Psi < 0$, clearly characterizes the left-handed writhe of the original double-stranded helical chain.

The results of Fig. 7 and Fig. 8 clearly indicate that the bending and writhing of the double-stranded helical chain are

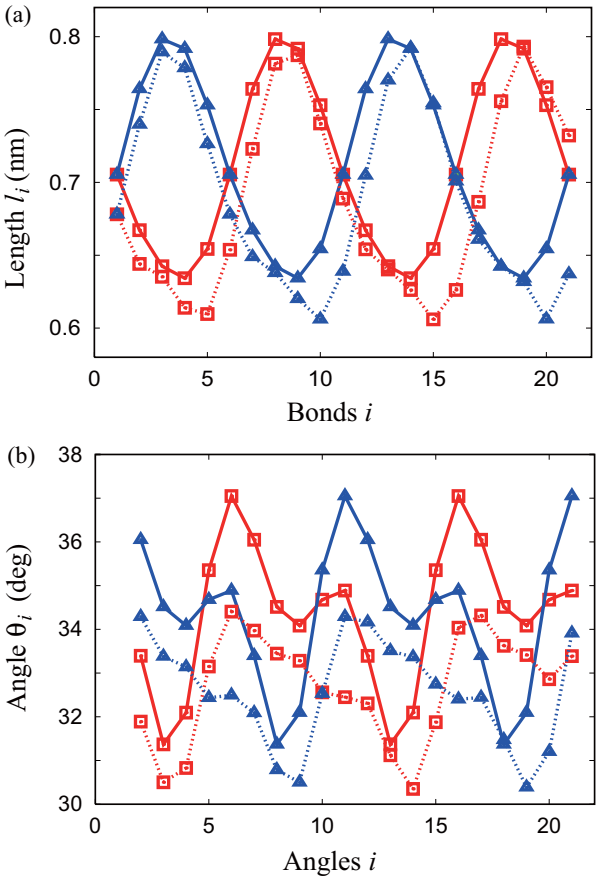

FIG. 6. (Color online) (a) Initial and final lengths of the respective bonds in the P and Q chains of the double-stranded helix, $l_i^{(P)}$ and $l_i^{(Q)}$ $(i = 1, \ldots, 21)$, for the structural relaxation shown in Fig. 3. The squares and triangles linked with *solid lines* represent the *initial* lengths of the respective bonds in the P chain or Q chain. The squares and triangles linked with *broken lines* represent the *final* lengths of the respective bonds in the P chain or Q chain. (b) Initial and final bending angles of the P and Q chains, $\theta_i^{(P)}$ and $\theta_i^{(Q)}$ $(i = 2, \ldots, 21)$, for the structural relaxation shown in Fig. 3. The squares and triangles linked with *solid lines* represent the *initial* values of the bending angles of the P chain or Q chain. The squares and triangles linked with *broken lines* represent the *final* values of the bending angles of the P chain or Q chain.

coupled in an asymmetric manner. These results justify the conjecture that the right-handed double-stranded helical chain tends to writhe in the left direction when it is bent as was postulated in our previous study on the wrapping of DNA [40]. Later in this paper, we demonstrate that the tendency of the right-handed double-stranded helical chain to writhe in the left direction upon bending can make the chain select left-handed wrapping around a core particle in a nucleosome.

Figure 9(a) shows the evolution of the total energy $E = E_{\text{bond}} + E_{\text{bend}}$ defined in Eq. (19) (solid curve), total bonding energy E_{bond} (broken curve), and total bending energy E_{bend} (dotted curve) of the double-stranded helical chain in the relaxation process of Fig. 7. The total energy decreases monotonically to zero since the process is a free relaxation process. In roughly the first 11 000 steps, the total bending energy decreases drastically while the total bonding energy

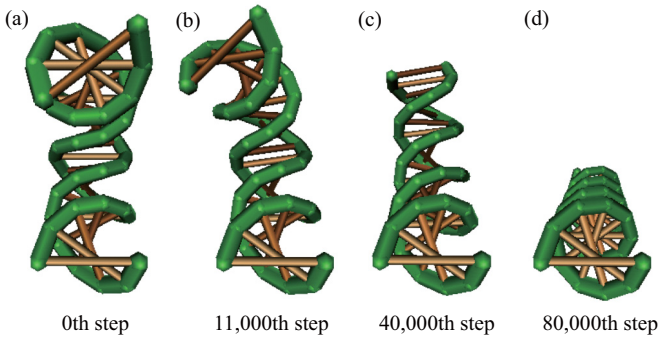

FIG. 7. (Color online) Structural relaxation of the double-stranded helical chain with $N = 22$ base pairs, where all the degrees of freedom of the model are allowed to relax. The chain is uniformly bent at the beginning as shown in (a). As the system relaxes, its conformation changes to (b) at the 11 000th step, to (c) at the 40 000th step, and eventually to (d) at the 80 000th step. The double-stranded helical chain *writhes in the left direction* in the course of this relaxation process as seen in (b).

does not change largely. These steps correspond to the conformational change from Fig. 7(a) to Fig. 7(b). Therefore, one can see that the writhing of the double-stranded helical chain in the left direction occurs during the process of relaxing the initial bending stress of the P and Q chains.

Figure 9(b) shows the evolution of the twisting number defined by Eq. (20) for the relaxation process of Fig. 7. We see

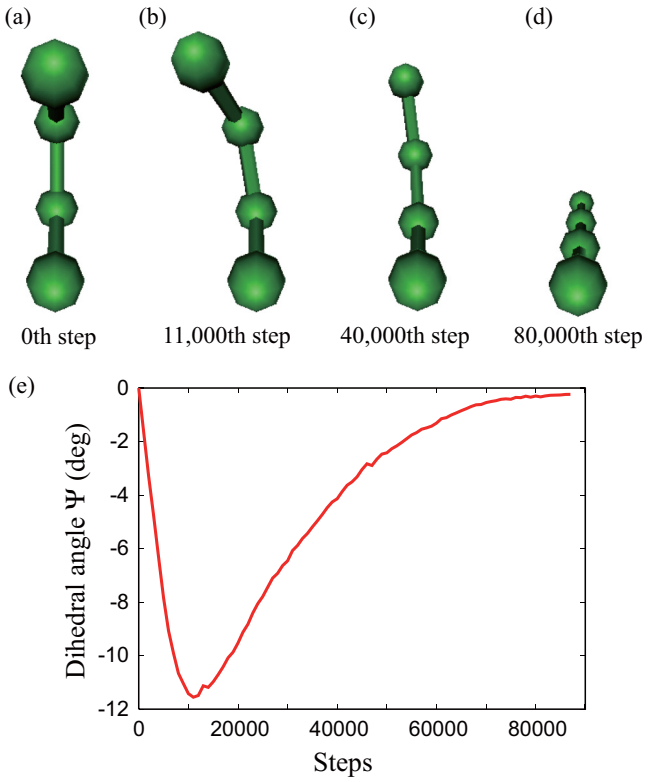

FIG. 8. (Color online) [(a)–(d)] Structural changes of the coarse-grained system of the double-stranded helical chain for the same relaxation process as in Figs. 7(a)–7(d). (e) Evolution of the dihedral angle of the coarse-grained system Ψ in the process of (a)–(d).

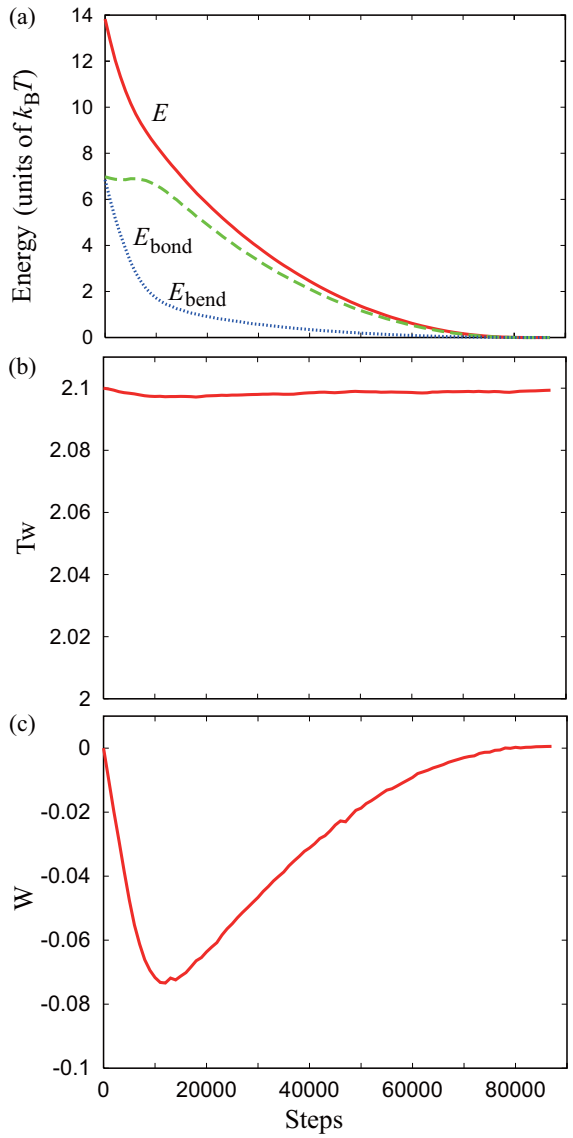

FIG. 9. (Color online) (a) Evolution of the total energy $E = E_{bond} + E_{bend}$ defined in Eq. (19) (solid curve), total bonding energy E_{bond} (broken curve), and total bending energy E_{bend} (dotted curve) of the double-stranded helical chain in the relaxation process of Fig. 7. (b) Evolution of the twisting number defined in Eq. (20). (c) Evolution of the writhing number defined in Eq. (21).

that the twisting number does not change very largely in this relaxation process as compared to the process of Fig. 3 [see Fig. 4(b)]. Figure 9(c) shows the evolution of the sum of the dihedral angles of the central backbone,

$$W = \sum_{i=2}^{N-2} \Phi_i/360^\circ, \tag{21}$$

which serves as a measure of the degree of writhing of the system. This quantity decreases in the negative direction from zero in roughly the first 11 000 steps, characterizing the writhing of the system in the left direction.

In order to confirm the robustness and generality of the left-handed writhing of the double-stranded helical chain upon bending, we carried out similar numerical experiments to Fig. 7 for different values of the force constants, k_{bond} and k_{bend}. We used the double-stranded helical chain with $N = 22$ base pairs. Initially, all the bending angles and dihedral angles of the central backbone were set to $\Theta_i = 10^\circ$ and $\Phi_i = 0^\circ$ (for all i), respectively. We then let the system relax freely in the same manner as in Fig. 7 and observed the evolution of the dihedral angle of the corresponding coarse-grained system, Ψ, which is defined in the same manner as in Fig. 8. Figure 10(a) shows the evolutions of Ψ of the double-stranded helical chain whose force constant for bonding is $k_{bond} = 100$ nm^{-2} and that for bending is $k_{bend} = 10, 50, 100, 200$ rad^{-2}, respectively, from the top to the bottom curves. We clearly see that the dihedral angle Ψ deviates always in the negative direction in the course of structural relaxation, indicating the left-handed writhing. The larger the force constant for bending is, the more largely the double-stranded helical chain writhes in the left direction. Thus we see that the bending stiffness of the two sugar-phosphate chains drives the left-handed writhing of the double-stranded helical chain upon bending. Figure 10(b) shows the evolutions of Ψ of the double-stranded helical chain whose force constant for bending is $k_{bend} = 100$ rad^{-2} and that for bonding is $k_{bond} = 10, 50, 100, 200$ nm^{-2}, respectively, from the bottom to the top curves. Again, we see that the dihedral angle Ψ deviates always in the negative direction in the course of structural relaxation, indicating the left-handed writhing. The larger the force constant for bonding is, the less the double-stranded helical chain writhes in the left direction. Thus we see that the bonding stiffness of the two sugar-phosphate chains hinders the left-handed writhing of the double-stranded helical chain upon bending. The results of Figs. 10(a) and 10(b) clearly indicate that the left-handed writhing of the double-stranded helical chain upon bending is a robust and general propensity resulted from the right-handed nature of the double-stranded helical chain.

Next, we investigate more in detail how the system relaxes its initial elastic stress by writhing in the left direction. The squares and triangles linked with the *solid lines* in Fig. 11(a) represent the *initial* lengths of the respective bonds in the P chain and Q chain, $l_i^{(P)} = |\mathbf{P}_{i+1} - \mathbf{P}_i|$ and $l_i^{(Q)} = |\mathbf{Q}_{i+1} - \mathbf{Q}_i|$ ($i = 1, \ldots, 21$), while the squares and triangles linked with the *broken lines* in the same figure represent the lengths of the bonds in the P chain and Q chain *at the* 11 000*th step*, which corresponds to Fig. 7(b). In the same manner, the squares and triangles linked with the *solid lines* in Fig. 11(b) represent the *initial* bending angles, $\theta_i^{(P)}$ and $\theta_i^{(Q)}$ ($i = 2, \ldots, 21$), of the two chains, while the squares and triangles linked with the *broken lines* in the same figure represent the bending angles of the two chains *at the* 11 000*th step*.

In Fig. 11(b), most of the bending angles of the two chains are larger than their equilibrium value $\theta_0 = 31.4^\circ$ at the beginning because of the bending of the central backbone of the double-stranded helical chain. This situation is exactly the same as in Fig. 6(b). After the first 11 000 steps, these bending angles decrease and approaches to the equilibrium value on average. The bond lengths shown in Fig. 11(a) also tend to decrease slightly in the first 11 000 steps. Thus, we see that the bending angles of the two chains relax largely and the contour length of the two chains decreases slightly when the system writhes in the left direction as in Fig. 7(b) starting from the planar conformation as in Fig. 7(a). It is noteworthy

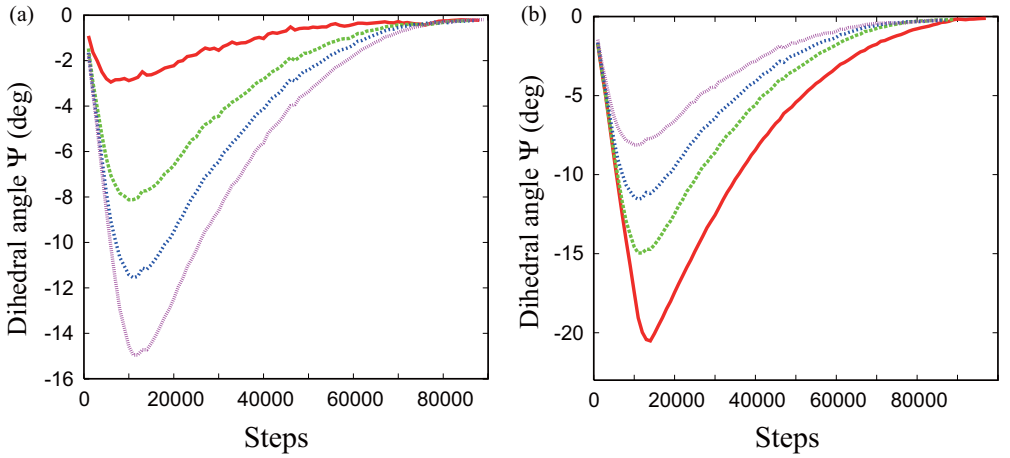

FIG. 10. (Color online) Evolutions of the dihedral angle, Ψ, of the coarse-grained system of the original double-stranded helical chain with $N = 22$ base pairs in the course of structural relaxation. Ψ is defined in the same manner as in Fig. 8. Panel (a) shows the evolutions of Ψ, where the force constant for bonding is $k_{\rm bond} = 100$ nm^{-2} and that for bending is $k_{\rm bend} = 10,\ 50,\ 100,\ 200$ rad^{-2} respectively from the top to the bottom curves. Panel (b) shows the evolutions of Ψ, where the force constant for bending is $k_{\rm bend} = 100$ rad^{-2} and that for bonding is $k_{\rm bond} = 10,\ 50,\ 100,\ 200$ nm^{-2}, respectively, from the bottom to the top curves.

that these behaviors of the bending angles and bond lengths of the two chains are quite similar to those observed in Fig. 6. In the next subsection, we semianalytically show that these behaviors of the bending angles and bond lengths can indeed be the origin for both the unwinding of the double-stranded helical chain and the left-handed writhing of the backbone of the chain.

C. A semianalytical account for the asymmetric couplings

We give here a semianalytical explanation for the numerical results presented in Sec. III A and in Sec. III B. We specifically focus on the mechanisms for the unwinding of the double-stranded helical chain upon bending as we have seen in Sec. III A and those for the left-handed writhing of the double-stranded helical chain upon bending as we have seen Sec. III B. Indeed, as we see below, these two mechanisms can be explained on the same footing.

Bending of the central backbone of the double-stranded helical chain generally increases the bending angles of the two constituent chains, $\theta_i^{(P)}$ and $\theta_i^{(Q)}$, on average as we have seen in Fig. 6(b) and in Fig. 11(b). As a result, once the double-stranded helical chain is bent, both of the two constituent chains respond to reduce their bending angles, $\theta_i^{(P)}$ and $\theta_i^{(Q)}$. Note here that if the two constituent chains assume more parallel conformations to the central backbone, the bending angles of these two chains, $\theta_i^{(P)}$ and $\theta_i^{(Q)}$, can become smaller. On the other hand, if the two constituent chains assume more perpendicular conformation to the central backbone on average, the bending angles of these two constituent chains, $\theta_i^{(P)}$ and $\theta_i^{(Q)}$, become larger. This can be understood by noting that an imaginary cylindrical surface around the central backbone where the two constituent chains lie has larger curvature in the perpendicular direction to the central backbone than in the parallel direction. Therefore, the two constituent chains tend to be more parallel to the central backbone on average when the central backbone of the double-stranded helical chain is bent. This tendency in turn forces the two constituent chains to *shrink* their contour lengths since the two constituent chains must stay intertwined around the central backbone whose contour length is fixed. We have indeed observed this shrinking of the two constituent chains in Fig. 6(a) and Fig. 11(a). Thus, in the following, we interpret this tendency of the two constituent chains to shrink their contour lengths upon bending in terms of the responses of twisting angles, $\{\varphi_i\}$, and writhing (dihedral) angles of the central backbone, $\{\Phi_i\}$. We then explain the numerical results of Sec. III A and of Sec. III B in terms of the responses of these angles.

As a measure of the contour length of each of the two constituent chains, we consider here the quantity $\sum_i |\mathbf{P}_i - \mathbf{P}_{i-1}|^2$ for the P chain and the quantity $\sum_i |\mathbf{Q}_i - \mathbf{Q}_{i-1}|^2$ for the Q chain. Here, the summations go over a single helical turn of the P and Q chains, respectively. In the following, we present an approximate expression for $\sum_i |\mathbf{Q}_i - \mathbf{Q}_{i-1}|^2$ for a uniformly bent conformation of the model DNA, i.e., $\Theta_i = \Theta$ (for all i), and investigate the responses of the twisting angles $\{\varphi_i\}$ and the dihedral angles $\{\Phi_i\}$. By symmetry, $\sum_i |\mathbf{P}_i - \mathbf{P}_{i-1}|^2$ of the P chain can be treated in the same manner. We will restrict ourselves to the regime where the amount of bending of the central backbone is small, i.e., $\Theta \ll 1$.

Based on Eq. (11), the bond vector $\mathbf{Q}_i - \mathbf{Q}_{i-1}$ is written as

$$\begin{aligned}\mathbf{Q}_i - \mathbf{Q}_{i-1} = \mathbf{r}_i - \mathbf{r}_{i-1} + \mathsf{R}_3^2(0,\Theta_2)\mathsf{R}_4^3(\Phi_2,\Theta_3)\cdots \\ \times \mathsf{R}_i^{i-1}(\Phi_{i-2},\Theta_{i-1})\mathbf{h}_i - \mathsf{R}_3^2(0,\Theta_2) \\ \times \mathsf{R}_4^3(\Phi_2,\Theta_3)\cdots\mathsf{R}_{i-1}^{i-2}(\Phi_{i-3},\Theta_{i-2})\mathbf{h}_{i-1}. \quad (22)\end{aligned}$$

Applying the condition that the central backbone of the double-stranded helical chain is uniformly bent, i.e., $\Theta_i = \Theta$ (for all i) to Eq. (22), and approximating as $\sin\Theta \cong \Theta$ and $\cos\Theta \cong 1$ based on the condition $\Theta \ll 1$, we obtain an approximate expression for the product of matrices

$\mathsf{R}_3^2(0,\Theta_2)\mathsf{R}_4^3(\Phi_2,\Theta_3)\cdots\mathsf{R}_i^{i-1}(\Phi_{i-2},\Theta_{i-1})$ as

$$\mathsf{R}_3^2(0,\Theta_2)\mathsf{R}_4^3(\Phi_2,\Theta_3)\cdots\mathsf{R}_i^{i-1}(\Phi_{i-2},\Theta_{i-1}) \cong \begin{bmatrix} \cos(i-3)\Phi & -\sin(i-3)\Phi & \Theta\sum_{k=1}^{i-3}\sin k\Phi \\ \sin(i-3)\Phi & \cos(i-3)\Phi & -\Theta\sum_{k=1}^{i-3}\cos k\Phi \\ \Theta\sum_{k=1}^{i-3}\sin k\Phi & \Theta\left(1+\sum_{k=1}^{i-3}\cos k\Phi\right) & 1 \end{bmatrix}, \tag{23}$$

where we also assumed that all the dihedral angles $\{\Phi_i\}$ of the central backbone are equal to Φ for simplicity based on the similarity of the dihedral angles. Application of Eq. (23) to Eq. (22) gives

$$\mathbf{Q}_i - \mathbf{Q}_{i-1} \cong \begin{pmatrix} d\Theta\sum_{k=1}^{i-3}\sin k\Phi + \sigma[\cos\{(i-3)\Phi+\varphi_i\} - \cos\{(i-4)\Phi+\varphi_{i-1}\}] \\ -d\Theta\sum_{k=1}^{i-3}\cos k\Phi + \sigma[\sin\{(i-3)\Phi+\varphi_i\} - \sin\{(i-4)\Phi+\varphi_{i-1}\}] \\ d + \sigma\Theta\left[\sum_{k=0}^{i-3}\sin(k\Phi+\varphi_i) - \sum_{k=0}^{i-4}\sin(k\Phi+\varphi_{i-1})\right] \end{pmatrix}. \tag{24}$$

Thus, we obtain

$$\begin{aligned} |\mathbf{Q}_i - \mathbf{Q}_{i-1}|^2 \cong{}& 4\sigma^2\sin^2\left(\frac{\Phi+\varphi_i-\varphi_{i-1}}{2}\right) + d^2 \\ &+ 2d\sigma\Theta[\sin\{(i-3)\Phi+\varphi_i\} \\ &- \sin\{(i-4)\Phi+\varphi_{i-1}\} - \sin(\Phi-\varphi_{i-1})]. \end{aligned} \tag{25}$$

We now consider the situation in which all the dihedral angles of the central backbone are constrained to zero, i.e., $\Phi = 0$, and the twist angles between any two neighboring base pairs take the same value, i.e., $\varphi_i - \varphi_{i-1} = \varphi$ (for all i), as in the initial conditions of the numerical experiment in Sec. III A. Then Eq. (25) reduces to

$$|\mathbf{Q}_i - \mathbf{Q}_{i-1}|^2 \cong 4\sigma^2\sin^2\left(\frac{\varphi}{2}\right) + d^2 + 2d\sigma\Theta\sin\{(i-1)\varphi\}. \tag{26}$$

The zeroth-order terms of Θ on the right-hand side of Eq. (26) correspond to (the square of) the average bond length [see Eq. (18)], while the first-order term of Θ represents the periodic deviation from the average as a function of the bond number i. Therefore, after summing Eq. (26) over a single period of the helical turn of the Q chain, the first-order term of Θ vanishes, and we obtain

$$\sum_{i=k}^{k+n-1}|\mathbf{Q}_i - \mathbf{Q}_{i-1}|^2 \cong 4n\sigma^2\sin^2\left(\frac{\varphi}{2}\right) + nd^2, \tag{27}$$

where k is an arbitrary number of the nodal point located at the beginning of the helical turn under consideration, and n is the number of base pairs per a single helical turn ($n = 2\pi/\varphi$). Since Eq. (27) is an increasing function of the twist angle φ for $0 < \varphi < \pi$, we see that φ must decrease in order to reduce the contour length of the Q chain around $\varphi = \varphi_0 = 36^\circ$. This explains why the double-stranded helical chain unwinds when the backbone of the chain is uniformly bent without writhe as we have seen in Sec. III A.

The asymmetric coupling between bending and writhing observed in Sec. III B can also be explained in the same manner as above based on Eq. (25). This time, we consider the differentiation (gradient) of the sum of Eq. (25) over a single helical turn of the Q chain with respect to the writhing angle Φ,

$$\begin{aligned} &\frac{\partial}{\partial\Phi}\sum_{i=k}^{k+n-1}|\mathbf{Q}_i - \mathbf{Q}_{i-1}|^2\Big|_{\Phi=0} \\ &= 2\sigma^2\sum_{i=k}^{k+n-1}\sin(\varphi_i - \varphi_{i-1}) \\ &\quad + 2\sigma d\Theta\sum_{i=k}^{k+n-1}(i-3)(\cos\varphi_i - \cos\varphi_{i-1}). \end{aligned} \tag{28}$$

Here, we have evaluated the quantity at $\Phi = 0$ since we are interested in the response of the system when it is uniformly bent without writhing as in the initial condition of the numerical experiment in Sec. III B. For the simplification of the right-hand side of Eq. (28), we now assume that the angles between any two neighboring base pairs take the same value, $\varphi_i - \varphi_{i-1} = \varphi_0$ (for all i), in view of the initial condition of the numerical experiment in Sec. III B. We then use the following relationships in order to simplify the second term of Eq. (28),

$$\sum_{i=k}^{k+n-1}\cos\varphi_i = \sum_{i=k}^{k+n-1}\cos\varphi_0(i-1) = 0, \tag{29}$$

$$\sum_{i=k}^{k+n-1}\cos\varphi_{i-1} = \sum_{i=k}^{k+n-1}\cos\varphi_0(i-2) = 0, \tag{30}$$

$$\begin{aligned} \sum_{i=k}^{k+n-1} i\cos\varphi_i &= \sum_{i=k}^{k+n-1} i\cos\varphi_0(i-1) \\ &\cong \int_k^{k+n} x\cos\left\{\frac{2\pi}{n}(x-1)\right\}dx \\ &= \frac{n^2}{2\pi}\sin\left\{\frac{2\pi}{n}(k-1)\right\}, \end{aligned} \tag{31}$$

$$\begin{aligned} \sum_{i=k}^{k+n-1} i\cos\varphi_{i-1} &= \sum_{i=k}^{k+n-1} i\cos\varphi_0(i-2) \\ &\cong \int_k^{k+n} x\cos\left\{\frac{2\pi}{n}(x-2)\right\}dx \\ &= \frac{n^2}{2\pi}\sin\left\{\frac{2\pi}{n}(k-2)\right\}. \end{aligned} \tag{32}$$

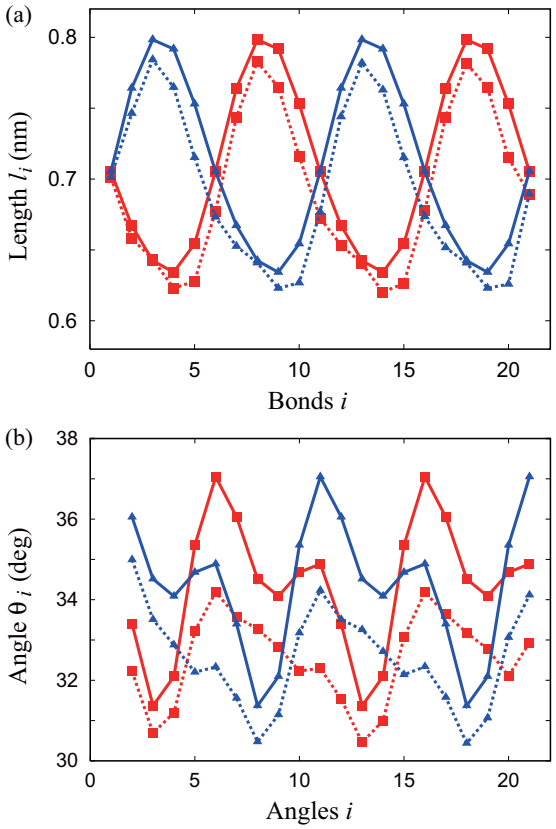

FIG. 11. (Color online) (a) Initial and intermediate (at the 11 000th step) lengths of the respective bonds in the P and Q chains of the double-stranded helical chain, $l_i^{(P)}$ and $l_i^{(Q)}$ ($i = 1, \ldots, 21$), in the relaxation process shown in Fig. 7. The squares and triangles linked with the *solid lines* represent the *initial* lengths of the respective bonds in the P chain and Q chain. The squares and triangles linked with the *broken lines* in the same figure represent the lengths of the bonds in the P chain and Q chain *at the* 11 000*th step*, which corresponds to Fig. 7(b). (b) Initial and intermediate (at the 11 000*th* step) values of the respective bending angles of the two chains, $\theta_i^{(P)}$ and $\theta_i^{(Q)}$ ($i = 2, \ldots, 21$), in the relaxation process shown in Fig. 7. The squares and triangles linked with the *solid lines* represent the *initial* values of the respective bending angles of the P chain and Q chain. The squares and triangles linked with the *broken lines* represent the values of the respective bending angles in the P chain and Q chain *at the* 11 000*th step*.

After applying Eq. (29)–(32) to Eq. (28), we obtain

$$\frac{\partial}{\partial \Phi} \sum_{i=k}^{k+n-1} |\mathbf{Q}_i - \mathbf{Q}_{i-1}|^2 \Bigg|_{\Phi=0} \cong 2\sigma^2 n \sin\varphi_0 + \frac{8\pi\sigma d\Theta}{\varphi_0^2} \sin\left(\frac{\varphi_0}{2}\right) \cos\left\{\frac{\varphi_0}{2}(2k-3)\right\}. \tag{33}$$

The first term on the right-hand side of Eq. (33) is a constant and is ≈ 11.76 nm^2 for the parameter values of the present model, $\sigma = 1$ nm, $\varphi_0 = 36^\circ$, and $n = 10$. The second term on the right-hand side of Eq. (33) is a periodic function of k, which varies within the range $\approx \pm 1.17$ nm^2 for the above parameter values of σ, φ_0, n, and $d = 0.34$ nm and $\Theta = 10^\circ$. Thus, Eq. (33) is positive, indicating that the sum of Eq. (25) over a single helical turn, or, equivalently, the chain length, is an increasing function of the writhing angle Φ around $\Phi = 0^\circ$ as in the initial condition of Sec. III B. This explains why the double-stranded helical chain writhes in the left direction ($\Phi < 0^\circ$) to shrink the total length of the P and Q chains upon bending.

Finally, it is interesting to consider the situation in which the chirality of the double-stranded helical chain is inverted: If the double strand of the chain is left handed, i.e., $\varphi_0 = -36^\circ$, Eq. (33) becomes negative. This indicates that if the double-stranded helical chain is left handed, the chain possesses the propensity to writhe in the right direction ($\Phi > 0^\circ$) to shrink the total length of the two constituent chains upon bending. This argument clearly indicates that the direction of writhing of the double-stranded helical chain is determined directly by the chirality of the double-stranded helix of the chain.

IV. CHIRAL SELECTION OF SUPERHELICAL AND WRAPPED STRUCTURES

In this section, we extend our analysis in the previous section to a longer segment of the double-stranded helical chain and gain insights into the mechanisms for the uniform left-handed wrapping of DNA in nucleosomes.

A. Chirality of a superhelix of the double-stranded helical chain

We take up here the same model of the double-stranded helical chain as in the previous sections with $N = 78$ base pairs and investigate its superhelical chirality. The double-stranded helical chain of this length is estimated to be slightly shorter than the DNA segment that can form a complete loop around a nucleosome core particle. We carry out structural relaxation simulations for this double-stranded helical chain in the same manner as in the previous section.

As the initial condition, all the bending angles of the central backbone of the model are set to $\Theta_i = 4.5^\circ$ ($i = 2, \ldots, 77$), and all the dihedral angles of the central backbone are set to zero, $\Phi_i = 0^\circ$ ($i = 2, \ldots, 76$). With this setting of the angles, the double-stranded helical chain forms a planar arc as shown in Fig. 12(a). The initial twisting angles of the double strand φ_i ($i = 1, \ldots, 78$) are set in accordance with Eq. (12). Such initial conformation of the double-stranded helical chain may

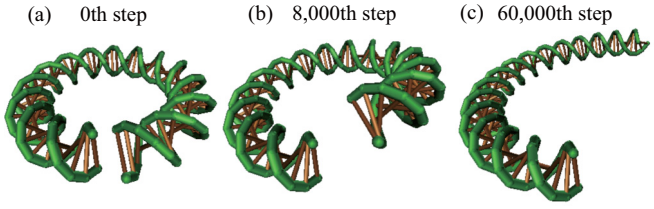

FIG. 12. (Color online) Relaxation of a long segment of the double-stranded helical chain with $N = 78$ base pairs. (a) The double-stranded helical chain segment initially forms a planar loop. (b) Then it quickly relaxes to a *left-handed* superhelical conformation after 8000 steps. (c) Finally, the superhelix slowly opens up and approaches the straight equilibrium conformation.

be realized when the chain is adsorbed on a core particle abruptly due to a strong attractive force.

Starting from this initial conformation, we let all the degrees of freedom of the double-stranded helical chain relax freely. That is, the bending angles $\{\Theta_i\}$, dihedral angles $\{\Phi_i\}$, and twisting angles $\{\varphi_i\}$ are changed little by little in the same manner as in the previous section so the total elastic energy of the system decreases monotonically. Once the relaxation starts, the planar loop of the double-stranded helical chain shown in Fig. 12(a) quickly deforms into a *left-handed* superhelical conformation as shown in Fig. 12(b) after 8000 steps. This transition from the planar loop to the left-handed superhelix is fast, indicating that the double-stranded helical chain has a propensity to form a left-handed superhelix. After this rapid conformational change, the superhelix slowly opens up and approaches the straight equilibrium conformation as shown in Fig. 12(c).

The result of Fig. 12 can be naturally understood by extending the result of Fig. 7. That is, the local propensity of a short segment of the double-stranded helical chain to writhe in the left direction upon bending observed in Fig. 7(b) gives rise to the global propensity of a longer segment of the double-stranded helical chain to form a left-handed superhelix.

In order to quantify the above preference of a bent segment of the double-stranded helical chain to form a left-handed superhelix, we computed the total energy of the chain as a function of the superhelical chirality of the model as shown in Fig. 13. In Figs. 13(a)–13(c), all the bending angles of the central backbone of the model are always fixed to $\Theta_i = 4.5^\circ$ ($i = 2, \ldots, 77$). Figures 13(a) and 13(b) show examples of the conformations of the system, where all the dihedral angles of the central backbone, $\{\Phi_i\}$, are set to $+0.5^\circ$ in Fig. 13(a) and to -0.5° in Fig. 13(b). As is clearly seen, the system assumes a right-handed superhelix when all the dihedral angles are positive, while the system assumes a left-handed superhelix when all the dihedral angles are negative. Figure 13(c) shows the total energy of the system as a function of the common value of the dihedral angles of the central backbone, where all the dihedral angles of the central backbone are set to the common value ranging from -2° to $+2^\circ$. It is evident from Fig. 13(c) that the energy profile is asymmetric with respect to the superhelical chirality of the system and has a minimum at the negative value of the dihedral angles around $\Phi_i = -0.4^\circ$. This clearly confirms the tendency of a bent segment of the double-stranded helical chain to form left-handed superhelices rather than right-handed ones.

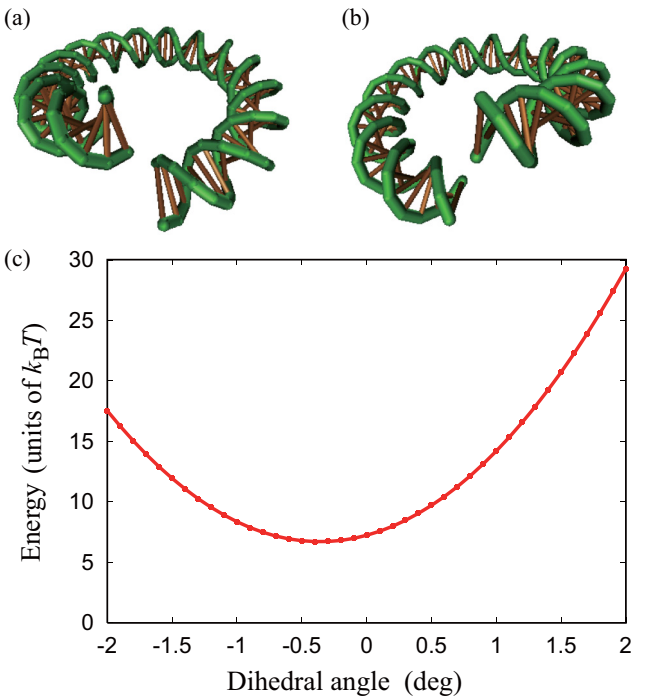

FIG. 13. (Color online) The double-stranded helical chain with $N = 78$ base pairs, where all the dihedral angles of the central backbone are set to $\Phi_i = +0.5^\circ$ ($i = 2, \ldots, 76$) in (a) and to $\Phi_i = -0.5^\circ$ ($i = 2, \ldots, 76$) in (b). (c) Total elastic energy of the double-stranded helical chain with $N = 78$ base pairs plotted as a function of the value of dihedral angles that is common to all the dihedral angles of the central backbone. In (a)–(c), the bending angles of the central backbone of the model are all set to $\Theta_i = 4.5^\circ$ ($i = 2, \ldots, 77$).

B. Implications for the chirality of wrapping of DNA in a nucleosome

The result of Sec. IV A implies a possible origin of the uniform left-handed wrapping of DNA around nucleosome core particles in nature. In order to demonstrate the implications, we introduce here a simple model of a nucleosome core particle and let our model of the double-stranded helical chain with $N = 78$ base pairs wrap around the core and relax. To model the attractive interaction between DNA and the core particle, we introduce a Morse potential between the core particle and each of the nodal points of the central backbone of the double-stranded helical chain. Thus, the total interaction energy between the double-stranded helical chain and the core particle is written as

$$\frac{V_{\rm core}}{k_{\rm B}T} = \sum_{i=1}^{N} \varepsilon_{\rm c} \exp\{-2\alpha_{\rm c}(|\boldsymbol{r}_i - \boldsymbol{r}_{\rm c}| - \sigma_{\rm c})\} - 2\varepsilon_{\rm c} \exp\{-\alpha_{\rm c}(|\boldsymbol{r}_i - \boldsymbol{r}_{\rm c}| - \sigma_{\rm c})\}, \quad (34)$$

where $N = 78$, $\boldsymbol{r}_{\rm c}$ is the center of the core particle and $\boldsymbol{r}_i$ is the position of i-th nodal point of the central backbone. The parameter $\varepsilon_{\rm c}$ determines the strength of the interaction between the core and the double-stranded helical chain, which is set to $\varepsilon_{\rm c} = 0.1$. The parameter $\alpha_{\rm c}$ determines the width of the well of the Morse potential and is set to $\alpha_{\rm c} = 2.0\,{\rm nm}^{-1}$. The parameter σ_c is the equilibrium distance between the center of the core and a nodal point of the backbone of the double-stranded helical chain. We determine the value of σ_c in accordance with the initial configuration of the system as follows.

The initial configuration of the model system is shown in Fig. 14(a), where double-stranded helical chain assumes exactly the same conformation as the initial conformation shown in Fig. 12(a). That is, the double-stranded helical chain is uniformly bent with all the bending angles $\Theta_i = 4.5^\circ$ ($i = 2, \ldots, 77$) and all the dihedral angles $\Phi_i = 0^\circ$ ($i = 2, \ldots, 76$) forming a planar loop. The initial twisting angles of the double strand φ_i ($i = 1, \ldots, 78$) are set in accordance with Eq. (12). The center of the core particle $\boldsymbol{r}_{\rm c}$ is initially placed at the center

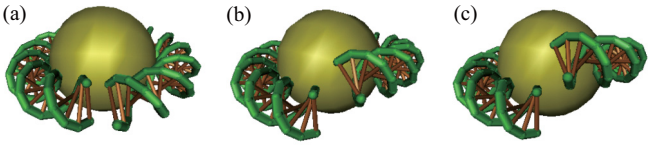

FIG. 14. (Color online) Structural relaxation of the system that consists of a spherical core particle and the double-stranded helical chain with $N = 78$ base pairs wrapped around the core. (a) Initial configuration of the system, where the double-stranded helical chain forms a planar loop around the core particle. (b) Final configuration of the system after full structural relaxation, where the double-stranded helical chain assumes a left-handed superhelical conformation around the core particle. (c) Final configuration of the system after full structural relaxation, where the force constant for bonding of the double-stranded helical chain is reduced to $k_{\rm bond} = 30\ {\rm nm}^{-2}$.

of the loop of the double-stranded helical chain. That is, the center of the core particle initially lie on the plane spanned by the central backbone of the model DNA and is equally distant from all the nodal points of the central backbone of the double-stranded helical chain. The equilibrium distance σ_c in Eq. (34) is set equal to the distance between each nodal point of the central backbone of the double-stranded helical chain and the center of the core at this initial configuration of the system. Thus σ_c is determined to be

$$\sigma_c = \frac{d/2}{\sin(4.5^\circ/2)} = 4.33\ {\rm nm}. \tag{35}$$

With this value of σ_c, the total interaction energy between the double-stranded helical chain and the core, $V_{\rm core}$, takes the minimum value at the initial configuration.

Starting from the initial configuration of the system as above, we carry out structural relaxation simulations. In this relaxation process, the bending angles Θ_i ($i = 2, \ldots, 77$), the dihedral angles Φ_i ($i = 2, \ldots, 76$), the twist angles φ_i ($i = 1, \ldots, 78$) of the model DNA, and the position of the center of the core particle are changed little by little and randomly so the total energy of the system decreases monotonically. Even though the interaction energy between the double-stranded helical chain and the core, $V_{\rm core}$ in Eq. (34), is minimum at the initial configuration, the system changes its overall configuration because the system relaxes the elastic stress inside the double-stranded helical chain at the expense of the interaction energy.

Figure 14(b) shows a final conformation of the system after the full relaxation, where the double-stranded helical chain has deformed into a left-handed superhelical conformation wrapped around the core particle. This result clearly indicates that the double-stranded helical chain can spontaneously select the left-handed wrapping around the core particle. The left-handed chirality of the wrapped structure in Fig. 14(b) may not be prominent enough in order for a longer segment to form the second turn around the core particle. Thus, in order to make the left-handed chirality of the wrapped segment clearer, we reduced the force constant for bonding $k_{\rm bond}$ from $k_{\rm bond} = 100\ {\rm nm}^{-2}$ to $k_{\rm bond} = 30\ {\rm nm}^{-2}$ to make the double-stranded helical chain more flexible. Figure 14(c) shows the final relaxed conformation of the system for this value of $k_{\rm bond} = 30\ {\rm nm}^{-2}$. As expected, Fig. 14(c) shows clearer left-handed chirality of wrapping than Fig. 14(b). In this way, the double-stranded helical chain can spontaneously select the left-handed wrapping around a nucleosome core particle.

Finally, it is interesting to discuss the roles of the size of the core particle in chiral selection in DNA wrapping. As demonstrated in Ref. [40], it is generally expected that chiral selectivity tends to decrease for wrapping around a larger core and tends to increase for wrapping around a smaller core. This is because wrapping around a smaller core generally induces larger bending of DNA, which can in turn drive asymmetric writhing of the backbone of DNA via a similar mechanism to the one presented in Sec. III C. Therefore, a smaller core would enhance chiral selectivity in the wrapping of DNA. However, wrapping around a smaller core generally requires larger bending energy in DNA, which tends to prevent full wrapping. Thus, it is expected that there exists an appropriate size of the core, which can balance both the chiral selectivity and the penalty on bending energy.

V. CONCLUDING REMARKS

We have reported asymmetric elasticity inherent in a right-handed double-stranded helical chain, which serves as a minimal model of biopolymers. It has been shown that a short segment of the double-stranded helical chain has a propensity to unwind when it is bent. It has also been shown that a short segment of the double-stranded helical chain has a propensity to writhe in the left direction upon bending. This propensity to writhe in the left direction gives rise to the propensity of a longer segment of the double-stranded helical chain to form a left-handed superhelix. Finally, we have demonstrated that such propensity of the double-stranded helical chain to form a left-handed superhelix can be a main factor for the uniform left-handed wrapping of DNA around nucleosome core particles in nature.

The propensity of the double-stranded helical chain to form a left-handed superhelix appears to be of great advantage for the systematic folding of DNA, in view of the fact that chromatin consists of various helical motifs of DNA with different scales. It is possible that if it were not for the propensity of DNA to select the proper chirality of coiling, DNA could easily get entangled in the course of folding. In nucleosomes, the core particles might play the essential role in provoking the propensity of DNA to writhe in the left direction by bending the backbone of DNA via the attractive interaction. Once DNA is attracted and bent by the core particle, DNA would spontaneously writhe in the left direction and selects the left-handed wrapping around the core particle as we have seen Sec. IV B. The uniformity of the left-handed wrapping of DNA in nucleosomes is also expected to be advantageous for organizing further higher-order structures in chromatin.

The results of the present study have implications on the existing theories and analysis of conformational dynamics of DNA: The propensity of the double-stranded helical chain to take the out-of-plane conformations rather than planar conformations (see Fig. 12) may have a non-negligible effect in cyclization of DNA [44,45]. Moreover, this propensity of DNA may play important roles in the packaging and ejection of viral DNA [46,47]. It is also possible that the asymmetric elasticity

of the present model of the double-stranded helical chain may be observed in more fine-scaled molecular dynamics simulations of DNA at the atomic level. In particular, the asymmetric properties of roll and slide and their coupling in DNA observed in the fine-scale studies in Refs. [28,48] may correspond to the asymmetric (chiral) coupling between bending and writhing in the present coarse-grained model of the double-stranded helical chain.

It is also interesting to extend the implications of the present study to other biopolymers than DNA. For example, it is known that an actin filament, which is a right-handed double-stranded helical chain, shows a propensity to form a left-handed superhelix when it slides on a track of heavy meromyosin [49]. This propensity of an actin filament seems to be consistent with the expectation deduced from the present model of the double-stranded helical chain. Since biopolymers are generally composed of chiral elements, such as amino acids and sugars, the bend-writhe coupling found in the present study may also play a significant role in the formation of suitable higher-order structures in biopolymers, including the morphology of bundles [50,51].

The numerical method for structural relaxation employed in the present study has been quite simple, in the sense that the method lowers the total elastic energy of the system monotonically. On the other hand, in reality, DNA and other biomolecules generally achieve their functions under thermal and noisy environments. Therefore, it would be an important next step to investigate conformational properties of the present model in the thermal and noisy environments by using Monte Carlo simulations or Langevin dynamics at appropriate temperatures. We expect that the propensity of the present model chain to form a left-handed superhelix still remains even under such thermal environment when the strength of the noise corresponds to the fluctuations at ambient temperatures. In addition, our initial results of Monte Carlo simulations at finite temperature indicate that thermal fluctuations even promotes the chiral selectivity of the present model chain provided that the strength of the thermal fluctuations is appropriate. This may also be explained in terms of the asymmetric coupling between bending and writhing of the model chain as has been described in the present paper: Thermal fluctuations can generally induce natural bending of the model chain. Although this bending is generally random and has no directionality, the coupling between bending and writhing leads to the tendency to the left-handed writhing of the backbone of the model chain. Based on these initial thoughts and results, we plan to scrutinize the significance of thermal fluctuations in the dynamics of helical chains in the near future.

It would also be an important next issue to obtain good estimates for the elastic force constants for bonding and bending, k_{bond} and k_{bend}, of the present model introduced in Eq. (13) and Eq. (14). In particular, in order for the present model to be a more realistic model of DNA, it would be important to incorporate and quantify stacking interactions among bases. To this end, detailed experimental data would be necessary. However, we wish to emphasize that the major results of the present study such as the propensities of the double-stranded helical chain to writhe in the left direction, to form left-handed superhelices, and to wrap in the left-handed manner are qualitatively independent of the values of the elastic force constants as we have seen in Fig. 5 and Fig. 10. This has been because the asymmetric (chiral) elasticities of the double-stranded helical chain reported in this paper are not due to the specific setting of the values of the elastic force constants but directly due to the right-handed helical chirality of the double-stranded chain. Moreover, the present study has indicated that if the double strand of the model chain were left handed, the chain would show the propensity to form a right-handed superhelix upon bending and to wrap around a core particle in a right-handed manner.

The present study has explored direct link between the lower-order chirality of the double-stranded helical chain and the higher-order chirality of the superhelix of the double-stranded chain. Since chromatin can be regarded as a nest of helical structures of DNA with different scales, it would be interesting to extend our present analysis to further higher-order helical structures in the hierarchy of chromatin. For example, it should be possible that the left-handed chirality of nucleosomes rules the chirality of the aggregates of nucleosomes such as the 30-nm fibers. Moreover, chirality of the 30-nm fibers could regulate the chirality of further higher-order helical structures in chromatin. In this way, the interaction between lower-order chirality and higher-order chirality could be a key factor for the true understanding of the designing principles of the hierarchical structure of chromatin.

ACKNOWLEDGMENTS

We are grateful to T. Iwaki, T. Sakaue, A. A. Zinchenko, S. Araki, Y. Higuchi, and M. Mikoshiba for fruitful discussions. We also thank H. Schiessel for stimulating discussions. We are also grateful to K. Takeyasu and K. Hizume for their valuable comments. We thank the anonymous referees for thoughtful comments and suggestions. T.Y. is grateful for the research opportunity at the Fukui Institute for Fundamental Chemistry, Kyoto University, for the initiation of the present study. T.Y. has been partially supported by JSPS Grants-in-Aid, No. 21840051 and No. 23740300, and by Waseda University Grant for SR 2012A-602, and by JST-CREST. K.Y. is supported by Grants-in-Aid, JSPS 23240044 and MEXT 25103012.

APPENDIX: ESTIMATION OF THE PERSISTENCE LENGTH OF THE MODEL

We present here an estimation of the bending persistence length of our model of the double-stranded helical chain based on the numerical results presented in this paper. In general, the bending persistence length of a polymer, l_p, is defined as the typical length scale along the contour of the polymer at which the tangent vectors of the polymer lose orientational correlation [42,43]. For a homopolymer consisting of segments of length b with bending rigidity (per a couple of neighboring segments) g, the persistence length l_p is related to the bending rigidity g as

$$l_p = \frac{gb}{k_{\mathrm{B}}T}, \tag{A1}$$

at temperature T.

As we see from the solid curve in Fig. 4(a), the double-stranded helical chain with $N = 22$ base pairs possesses the total energy of about $E = 10k_BT$–$14k_BT$ depending on the stages of structural relaxation. It should be noted that the bending angles of the central backbone of the double-stranded helical chain, Θ_i, are all fixed to $\Theta_i = 10^\circ = 0.174$ (rad) in the relaxation process of Fig. 4(a). By assuming the harmonic elasticity between the total energy E and the bending angle of the central backbone Θ_i, one can express E as

$$E = \tfrac{1}{2}g(N-1)\Theta_i^2. \tag{A2}$$

Therefore, the bending rigidity is estimated to be $g = 2E/(N-1)\Theta_i^2 = 34.35k_BT$, where we adopted the values of $E = 11k_BT$, $N = 22$, and $\Theta_i = 0.174$ (rad). After applying this value of g to Eq. (A1) and noting that $b = 0.34$ nm for our model, we obtain the persistence length as $l_p = 11.7$ nm.

[1] J. D. Watson, T. A. Baker, S. P. Bell, A. Gann, M. Levine, and R. Losick, *Molecular Biology of the Gene, Sixth Edition* (Pearson Education, San Francisco, 2008).
[2] B. Alberts, A. Johnson, J. Lewis, M. Raff, K. Roberts, and P. Walter, *Molecular Biology of the Cell, Fifth Edition* (Garland Science, New York, 2008).
[3] H. Schiessel, J. Phys.: Cond. Matt. **15**, R699 (2003).
[4] H. Schiessel, Eur. Phys. J. E **19**, 251 (2006).
[5] M. Depken and H. Schiessel, Biophys. J. **96**, 777 (2009).
[6] M. Emanuel, N. H. Radja, A. Henriksson, and H. Schiessel, Phys. Biol. **6**, 025008 (2009).
[7] G. Arya and T. Schlick, Proc. Natl. Acad. Sci. USA **103**, 16236 (2006).
[8] G. Arya, Q. Zhang, and T. Schlick, Biophys. J. **91**, 133 (2006).
[9] B. VS Iyer, M. Kenward, and G. Arya, BMC Biophys. **4**, 8 (2011).
[10] T. R. Strick, J.-F. Allemand, D. Bensimon, and V. Croquette, Biophys. J. **74**, 2016 (1998).
[11] J. F. Allemand, D. Bensimon, R. Lavery, and V. Croquette, Proc. Natl. Acad. Sci. U.S.A. **95**, 14152 (1998).
[12] S. Neukirch, Phys. Rev. Lett. **93**, 198107 (2004).
[13] J. Gore, Z. Bryant, M. Nöllmann, M. U. Le, N. R. Cozzarelli, and C. Bustamante, Nature **442**, 836 (2006).
[14] T. Lionnet, S. Joubaud, R. Lavery, D. Bensimon, and V. Croquette, Phys. Rev. Lett. **96**, 178102 (2006).
[15] J. F. Marko, Phys. Rev. E **76**, 021926 (2007).
[16] J. F. Marko and E. D. Siggia, Macromolecules **27**, 981 (1994).
[17] I. M. Kulić, D. Andrienko, and M. Deserno, Europhys. Lett. **67**, 418 (2004).
[18] Y. S. Velichko, K. Yoshikawa, and A. R. Khokhlov, Biomacromolecules **1**, 459 (2000).
[19] Y. S. Velichko, K. Yoshikawa, and A. R. Khokhlov, Comp. Phys. Comm. **146**, 122 (2002).
[20] K. Besteman, S. Hage, N. H. Dekker, and S. G. Lemay, Phys. Rev. Lett. **98**, 058103 (2007).
[21] I. V. Dobrovolskaia, M. Kenward, and G. Arya, Biophys. J. **99**, 3355 (2010).
[22] Y. Higuchi, T. Sakaue, and K. Yoshikawa, Phys. Rev. E **82**, 031909 (2010).
[23] A. A. Kornyshev and S. Leikin, Phys. Rev. Lett. **84**, 2537 (2000).
[24] A. G. Cherstvy, J. Phys. Chem. B **112**, 12585 (2008).
[25] K. Luger, A. W. Mäder, R. K. Richmond, D. F. Sargent, and T. J. Richmond, Nature **389**, 251 (1997).
[26] T. J. Richmond and C. A. Davey, Nature **423**, 145 (2003).
[27] M. Y. Tolstorukov, A. V. Colasanti, D. M. McCandlish, W. K. Olson, and V. B. Zhurkin, J. Mol. Biol. **371**, 725 (2007).
[28] W. K. Olson and V. B. Zhurkin, Curr. Opin. Struct. Biol. **21**, 348 (2011).
[29] E. J. Sambriski, D. C. Schwartz, and J. J. de Pablo, Biophys. J. **96**, 1675 (2009).
[30] A. K. Dasanna, N. Destainville, J. Palmeri, and M. Manghi, Europhys. Lett. **98**, 38002 (2012).
[31] J. Palmeri, M. Manghi, and N. Destainville, Phys. Rev. Lett. **99**, 088103 (2007).
[32] J. Yan and J. F. Marko, Phys. Rev. Lett. **93**, 108108 (2004).
[33] R. M. Fye and C. J. Benham, Phys. Rev. E **59**, 3408 (1999).
[34] M. Tanaka, J. Phys. Condens. Matter. **16**, S2127 (2004).
[35] K. Besteman, K. Van Eijk, and S. G. Lemay, Nat. Phys. **3**, 641 (2007).
[36] A. A. Zinchenko, K. Yoshikawa, and D. Baigl, Phys. Rev. Lett. **95**, 228101 (2005).
[37] A. A. Zinchenko, T. Sakaue, S. Araki, K. Yoshikawa, and D. Baigl, J. Phys. Chem. **111**, 3019 (2007).
[38] A. Hamiche, V. Carot, M. Alilat, F. De Lucia, M.-F. O'Donohue, B. Révet, and A. Prunell, Proc. Natl. Acad. Sci. USA **93**, 7588 (1996).
[39] W. Li, S.-X. Dou, and P.-Y. Wang, J. Theor. Biol. **235**, 365 (2005).
[40] T. Yanao and K. Yoshikawa, Phys. Rev. E **77**, 021904 (2008).
[41] A. Patriciu, G. S. Chirikjian, and R. V. Pappu, J. Chem. Phys. **121**, 12708 (2004).
[42] P. A. Wiggins and P. C. Nelson, Phys. Rev. E **73**, 031906 (2006).
[43] S. Geggier and A. Vologodskii, Proc. Natl. Acad. Sci. USA **107**, 15421 (2010).
[44] D. Shore, J. Langowski, and R. L. Baldwin, Proc. Natl. Acad. Sci. USA **78**, 4833 (1981).
[45] L. Czapla, D. Swigon, and W. K. Olson, J. Chem. Theory Comput. **2**, 685 (2006).
[46] P. K. Purohit, M. M. Inamdar, P. D. Grayson, T. M. Squires, J. Kondev, and R. Phillips, Biophys. J. **88**, 851 (2005).
[47] H. G. Garcia, P. Grayson, L. Han, M. Inamdar, J. Kondev, P. C. Nelson, R. Phillips, J. Widom, and P. A. Wiggins, Biopolymers **85**, 115 (2006).
[48] R. Lavery, K. Zakrzewska *et al.*, Nucl. Acids Res. **38**, 299 (2009).
[49] T. Nishizaka, T. Yagi, Y. Tanaka, and S. Ishiwata, Nature **361**, 269 (1993).
[50] C. Heussinger, M. Bathe, and E. Frey, Phys. Rev. Lett. **99**, 048101 (2007).
[51] C. Heussinger, F. Schüller, and E. Frey, Phys. Rev. E **81**, 021904 (2010).